Force-displacement relationship modelling of masonry infilled walls with openings in hinged steel frames

Haoran Zuo (haoran.zuo@polyu.edu.hk)
The Hong Kong Polytechnic University
Weiping Zhang
Tongji University College of Civil Engineering
Baotong Wang
Tongji University College of Civil Engineering
Xianglin Gu
Tongji University College of Civil Engineering

Research Article

Keywords: Force-displacement relationship, masonry infill, aspect ratio, vertical load, opening, hinged steel frame

Posted Date: April 30th, 2021

DOI: https://doi.org/10.21203/rs.3.rs-460695/v1

Force-displacement relationship modelling of masonry infilled walls with openings in hinged steel frames

Haoran Zuo, Weiping Zhang*, Baotong Wang, Xianglin Gu

Key Laboratory of Performance Evolution and Control for Engineering Structures of Ministry of Education, Tongji University, Shanghai, 200092, China

**Corresponding author*

E-mail address: weiping_zh@tongji.edu.cn (W. Zhang)

ABSTRACT

Seismic behaviour of masonry infilled frames has attracted extensive attentions from researchers, and it was found that infills normally experienced a diagonal compression under lateral loading. Infill was therefore assumed as an equivalent diagonal strut in structural response estimations of infilled frames, and a force-displacement curve was adopted to describe the mechanical properties of the strut. However, the influences of infill aspect ratio, vertical load acting on the surrounding frames, and opening were not systematically addressed in establishing the force-displacement relationship of infills. To investigate the effects of these influential parameters on the lateral responses of infilled walls including initial stiffness and strength, detailed three-dimensional finite element (FE) models of masonry infilled hinged steel frames are developed in ABAQUS in the present study, and a wide parametric study with respect to various aspect ratios, vertical loads, and opening sizes and locations is performed. A generalized force-displacement relationship model of infilled walls is proposed based on regression analyses of numerical results. The efficacy of the proposed model is examined by using the existing experimental test results, and it shows that the model can accurately predict the lateral stiffness and load carrying capacity of infilled walls and thus has great potential applications in structural designs and analyses for masonry infilled steel frames.

Keywords: Force-displacement relationship, masonry infill, aspect ratio, vertical load, opening, hinged steel frame

1. Introduction

Masonry infills are commonly used as either interior partitions or exterior claddings in reinforced concrete (RC) and steel framed structures, which are still the widespread structural types around the world. Due to the unpredictable failure characteristics and highly variable material properties of masonry infills, they are only considered as gravity loads in the current design practices, and the surrounding frames are designed

against external excitations such as wind and seismic loads by neglecting the interaction between the infills and bounding frames. However, the expected behaviour of framed structures, namely seismic demand, seismic capacity, and failure modes, could be significantly changed by the presence of infills. Therefore, simplifying the frames and infills as structural and non-structural elements cannot accurately capture the effects induced by the infills, and it is important and necessary to implement a comprehensive study on the structural responses of framed structures considering the influences of infilled walls.

Over the past several decades, extensive experimental research works have been carried out to investigate the seismic behaviour of infilled frames especially for RC structures (e.g., (Alwashali et al. 2019; Cavaleri and Di Trapani 2014; Morandi et al. 2018)). In the experimental tests of infilled steel frames, some influential parameters were studied, and the test results showed that the structural stiffness and strength were significantly related to the rigidity of the steel beam-column connection (Mohammadi and Emami 2019) and the connection type between the infill and frame (Liu and Manesh 2013). In addition, infilled steel frames with different masonry brick types exhibited different behaviours with respect to the lateral stiffness, load carrying capacity, and energy dissipation capacity (Markulak et al. 2013). Similar to infilled RC frames (Shing and Mehrabi 2002), El-Dakhakhni et al. (2003) summarized five possible failure modes of infilled steel frames, and only the corner crushing and sliding shear failure modes were of practical importance.

Instead of conducting experimental tests, some researchers adopted numerical methods to estimate the seismic responses of framed structures with infills. These methods are referred to as micro- (Asteris et al. 2013) and macro-modelling (Asteris et al. 2011; Di Trapani et al. 2015) strategies. In the micro-modelling approach (Asteris et al. 2013), the masonry bricks and mortar joints were explicitly modelled, or the infill was assumed as a homogeneous and isotropic continuum. This approach can simulate both the global structural responses of infilled frames and the local damages (e.g., cracks) of infills under the lateral loading by sacrificing large computational time, which would hinder its wide applications in the structural analyses and designs of infilled frames.

On the other hand, it has been recognized that the infill mainly experiences a compression along the diagonal direction under the lateral load. Polyakov (1960) proposed an idea that using an equivalent diagonal strut to represent the infill, which can be deemed as a macro-modelling approach to consider the infill effects (Asteris et al. 2011; Di Trapani et al. 2015) and have been adopted in the structural response analyses of infilled frames (e.g., (Cavaleri et al. 2017; Gentile et al. 2019; Perrone et al. 2017)). In the macro-modelling approach (i.e., the diagonal strut model), the critical parameter is the determination of the strut width, and different researchers proposed different formulas to calculate the strut width (Klingner and Bertero 1978; Liauw and Kwan 1984; Mainstone 1971). However, a constant strut width cannot consider

the stiffness and strength variations of infills with increasing the lateral load, and a force-displacement curve is required to fully describe the stiffness and strength softening during the whole loading process (Benavent-Climent et al. 2018; Cavaleri and Di Trapani 2014; Di Trapani et al. 2020; Dolšek and Fajfar 2008; Uva et al. 2012a, b).

In the development of the force-displacement relationship of the diagonal strut, it should be noted that the influences of infill aspect ratio, vertical load on the structure, and opening were less researched. Papia et al. (2003) used an equivalent criterion between the initial stiffness of the actual infilled frame and of the diagonal strut model to calculate the strut width, and they concluded that the strut width was associated with the infill aspect ratio although only two different aspect ratios (1.0 and 1.5) were investigated in their study. Regarding the effect of vertical load on the in-plane behaviour of infilled frames, the axial load could increase the initial stiffness and structural strength while decrease the structural ductility, which has experimentally confirmed by Liu and Manesh (2013). Later, Campione et al. (2015), and Chen and Liu (2016) quantified the effect of vertical load on the initial stiffness and lateral resistance of infilled walls. Furthermore, the openings like windows and doors are usually designed in infills for architectural functions, and it has been demonstrated that the openings could reduce the lateral stiffness and strength of infilled frames (Kakaletsis and Karayannis 2008; Morandi et al. 2018). Tasnimi and Mohebkhah (2011) used the reduction factors to consider the influence of opening, which normally can be obtained from the statistical regression analyses of experimental test results (Humayun Basha et al. 2020; Mohammadi and Nikfar 2013). However, only the central openings were investigated in the above-mentioned studies (Humayun Basha et al. 2020; Mohammadi and Nikfar 2013; Tasnimi and Mohebkhah 2011). Chen and Liu (2015) performed a parametric study to investigate the influences of opening size and location on the in-plane behaviour of infilled steel frames, and the numerical results showed that the degree of the reduction on the lateral stiffness and strength of infilled walls was related to the opening size as well as the opening location. To the best knowledge of the authors, the combined influences of infill aspect ratio, vertical load, and opening size and location on the force-displacement relationship of infills have not been reported in the open literature.

In a companion paper of the authors (Zuo et al. 2021), the in-plane behaviour of masonry infilled hinged steel frames (MIHSFs) without and with openings were investigated under cyclic loading tests, and three-dimensional (3D) finite element (FE) models of the test specimens were developed in ABAQUS. As an extension of that work, the present study aims to further conduct a comprehensive study to investigate the effects of infill aspect ratio, vertical load and opening on the in-plane responses of infilled walls in hinged steel frames (HSFs), and a generalized force-displacement relationship model for infills will be proposed based on regression analyses of numerical results, which will be validated using the available experimental test results.

2. Brief review of FE model

The prototype structure of MIHSFs adopted in the present study is a historical building in Shanghai, China, and its detailed information can be found in Gu et al. (2018), which is not repetitively introduced here for conciseness. Moreover, the FE models of 1/2 scaled MIHSFs were developed and validated in the authors' previous study (Zuo et al. 2021), and they are briefly reviewed in this section for the sake of completeness.

Solid elements (C3D8R element) are used to model the surrounding frame including the steel beam, steel columns, T-shaped concrete beam and masonry columns, and the concrete foundation beam. For the infilled wall, a simplified micro-modelling technique is adopted where the infilled wall is homogenized as one-phase material and modelled by the continuum elements (C3D8R element) instead of developing the clay bricks and mortar joints explicitly. This modelling approach is adopted because the primary objective of the present study is to investigate the global response (i.e., the lateral force-displacement relationship) of the infilled wall under the lateral load, and a high-fidelity FE model is normally required when the local response (e.g., crack pattern) of the infilled wall is of interest. Fig. 1 shows a schematic of the FE model of MIHSFs.

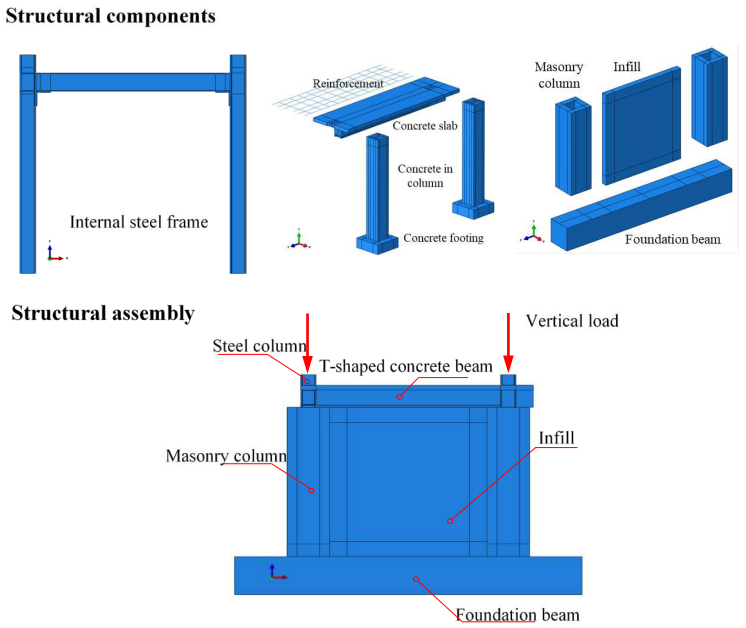

Fig. 1. FE model of MIHSFs

A normal contact and a tangential contact are adopted to model the interaction between the infill and bounding frame in the FE models. The normal contact behaviour is simulated by a hard contact in ABAQUS, in which the surfaces of the infill and frame can separate without any tensile resistance while the compressive forces will be generated when the surfaces are in a tight contact. In addition, the Coulomb

118 friction is defined to model the tangential contact behaviour between the infill and frame, and the friction
119 coefficient is set as 0.7 (GB50003 2011).

120 The nonlinear behaviour of concrete and masonry materials can be described by using the concrete damage
121 plasticity (CDP) model in ABAQUS. In the CDP model, the plasticity parameters (ψ, e, σ_{b0}/σ_{c0}, K_c, and μ)
122 and the uniaxial constitutive laws in compression and tension are needed. The values of the plasticity
123 parameters recommended in other literature (e.g., (Li et al. 2019)) are adopted in the present study, which
124 are 30, 0.1, 1.16, 0.6667, and 0.0001, respectively. The compressive and tensile stress-strain relationships
125 of the concrete and masonry materials are obtained from the design codes of concrete and masonry
126 structures (GB50010 2010; GB50003 2011), and Table 1 tabulates the compressive strength and Young's
127 modulus of the concrete and masonry materials.

128 As for the steel material, the Young's modulus and tensile stress-strain curve are defined to model its elastic
129 and plastic behaviour, which are measured from the material testing, and a Poisson ratio of 0.3 is also
130 defined. The characteristic strengths and elastic modulus of the steel material are also given in Table 1. It
131 should be noted that the values in this table are the average results of three measured samples, and the
132 elastic modulus of rebar is abnormally lower than that of steel frame; however, which are in the concrete
133 slab, and the structural responses are mainly governed by the steel frame and infilled wall.

134 **Table 1** Material properties of concrete, masonry and steel (Gu et al. 2018)

Material	Compressive strength (MPa)	Shear bond strength (MPa)	Elastic modulus ($\times 10^4$ MPa)
Concrete	18.6	-	2.5
Masonry	2.95	0.27	0.34
Material	Yield strength (MPa)	Ultimate strength (MPa)	Elastic modulus ($\times 10^5$ MPa)
Steel beam	274	385	1.82
Steel column	261	374	1.73
Steel plate	278	442	2.18
Rebar	281	476	1.61

135

136 In the FE models, all the degrees-of-freedom of the foundation beam are restricted to simulate the fixed
137 boundary condition in practice. To investigate the in-plane responses of MIHSFs, three loading steps are
138 defined, which are the gravity, axial, and lateral loads, respectively. A gravitational acceleration of 9.8 m/s^2
139 is applied to consider the self-weight of MIHSFs; a surface pressure is loaded at the top of each column to
140 simulate the axial load acting on the surrounding frames; and a displacement-controlled lateral load of 50
141 mm is imposed to the FE models.

142

143

3. Parametric study

To systematically investigate the influences of the infill aspect ratio (a ratio of the infill length l_w to the infill height h_w), vertical load, and opening size and location on the lateral responses of infilled walls, a parametric study is conducted. The material properties, constitutive laws, boundary conditions, and analysis procedures in this parametric study are the same as those introduced in Section 2. Moreover, it needs to clarify that the relative stiffness of bounding frames also affects the in-plane behaviour of infilled walls, which has been comprehensively examined in the previous studies (e.g., (Cavaleri et al. 2005; Papia et al. 2003)) and will be presented in the following section, therefore, the geometric dimensions of boundary elements (beams and columns) are not considered as variable parameters in this section.

3.1. Effect of infill aspect ratio

Considering the actual infill aspect ratio in the prototype structure, in total 15 different infill aspect ratios are designed, which are listed in Table 2. As tabulated, the infill aspect ratio is in a range of [0.48, 2.15], and only the infill length is changed while keeping the infill height as a constant value of 2000 mm. Note that the lateral load-displacement curves of infilled walls are obtained by subtracting the lateral responses of the bare frames (BFs) from those of MIHSFs. Therefore, 30 different FE models (15 solid infilled frames plus 15 BFs) are analysed under a monotonic lateral loading.

Table 2 Designed FE models with different infill aspect ratios

Model No.	Length l_w (mm)	Height h_w (mm)	Aspect ratio (l_w/h_w)
S_1	950	2000	0.48
S_2	1050	2000	0.53
S_3	1150	2000	0.58
S_4	1250	2000	0.63
S_5	1350	2000	0.68
S_6	1550	2000	0.78
S_7	1800	2000	0.90
S_8	2000	2000	1.00
S_9	2200	2000	1.10
S_10	2400	2000	1.20
S_11	2600	2000	1.30
S_12	2800	2000	1.40
S_13	3300	2000	1.65
S_14	3800	2000	1.90
S_15	4300	2000	2.15

Note: S denotes solid infill in Table 2.

Fig. 2 shows the lateral load-displacement curves of BFs, MIHSFs and infilled walls under different infill aspect ratios. As shown in Fig. 2(a), the lateral responses of BFs are almost the same regardless of the infill aspect ratio due to the pin-hinged connection between the beam and columns, and only the results of five different infill aspect ratios are thus presented to show the curves much clearer. However, the infill aspect

ratio has a significant influence on the lateral responses of MIHSFs. As shown in Fig. 2(b), the initial stiffness of MIHSFs increases with increasing the infill aspect ratio, and the lateral load resistance of MIHSFs also increases when the infill aspect ratio is smaller than 1.20, but the increment is not evident when the infill aspect ratio is larger than 1.20. These obvious differences in terms of the initial stiffness and lateral load resistance of MIHSFs are caused by the diverse lateral behaviour exhibited by the infilled walls with different infill aspect ratios. As can be seen in Fig. 2(c), the lateral load-displacement curves of infilled walls mainly consist of three stages. In the first stage, the infilled wall is in a linear elastic behaviour, and the lateral load of the infilled wall increases linearly with the imposed displacement, then it increases nonlinearly due to the stiffness degradation. After the lateral load carrying capacity of the infilled wall is reached, the infilled wall is severely damaged, which leads to the occurrence of the descending branch in the lateral load-displacement curve of the infilled wall.

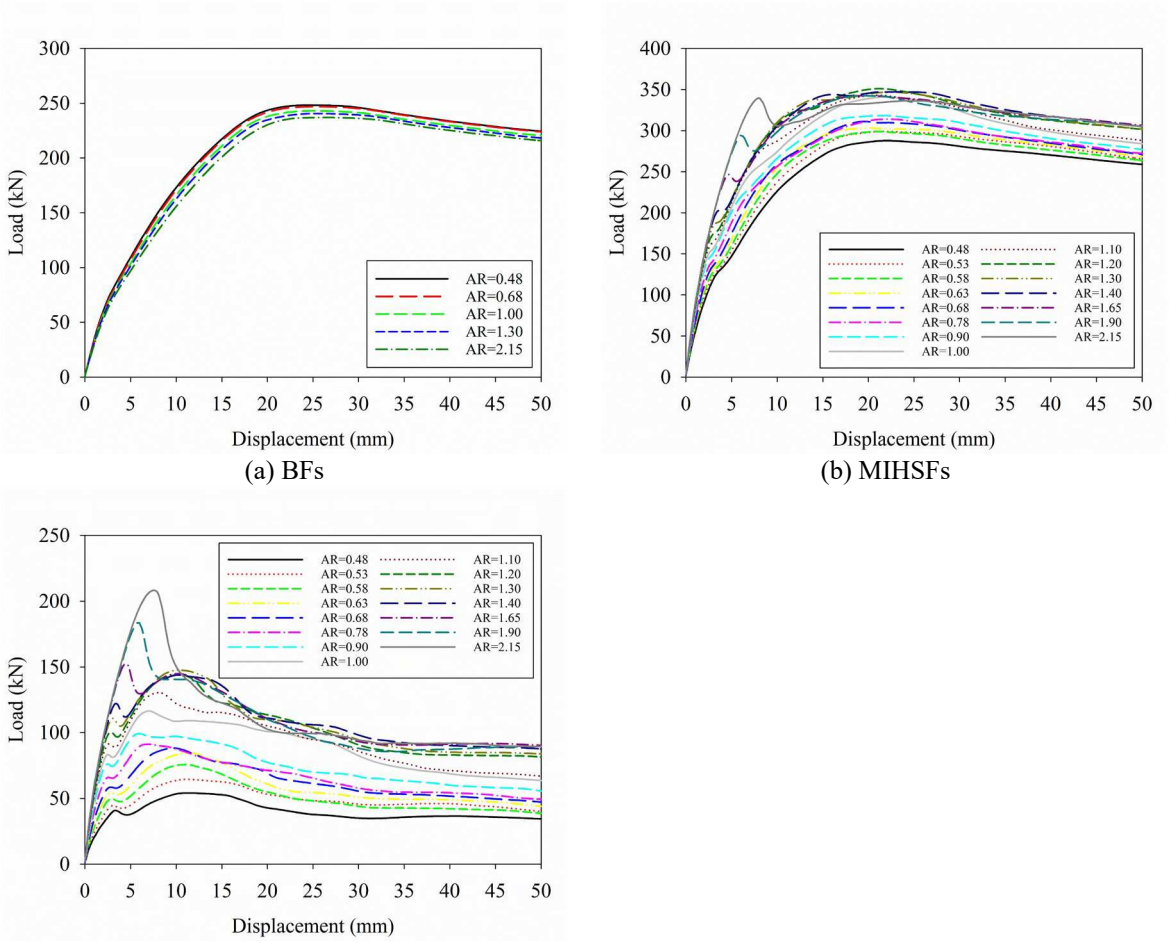

(a) BFs (b) MIHSFs

(c) Infilled walls

Fig. 2. Lateral load-displacement curves of BFs, MIHSFs and infills with different aspect ratios

Fig. 3 shows the initial stiffness, maximum lateral load and net load of infilled walls with different aspect ratios. In which, the net load is computed by subtracting the corresponding load of BF from the lateral load

carrying capacity of MIHSF at the same displacement. As shown, the initial stiffness and maximum lateral load of the infilled walls increase with increasing the infill aspect ratio, however, the net load carried by the infilled walls increases when the infill aspect ratio is smaller than 1.20, and it reaches a stable value when the infill aspect ratio is larger than 1.20. This is due to the stable lateral responses of the bare and infilled frames when the infill aspect ratio is over 1.20 as shown in Figs. 2(a) and (b).

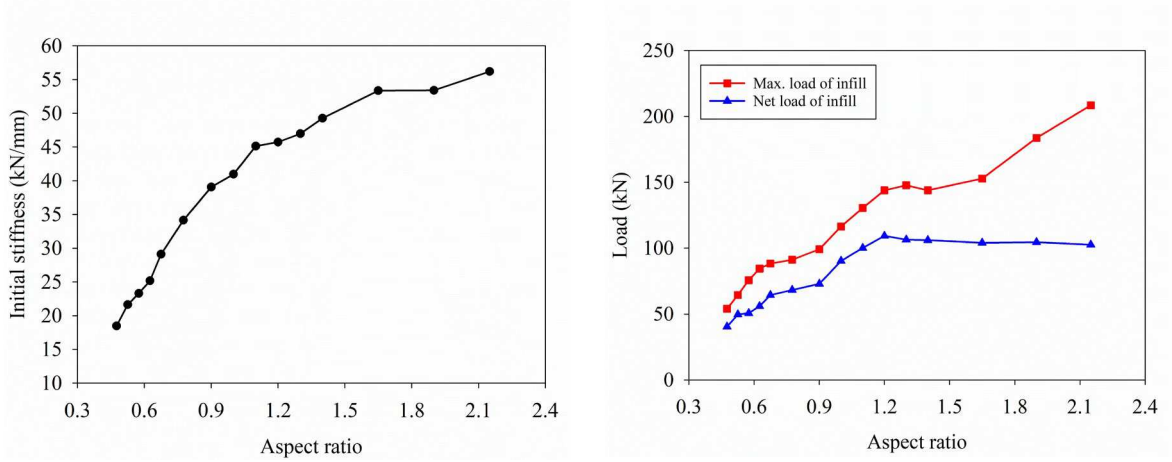

(a) Initial stiffness (b) Maximum and net loads

Fig. 3. Initial stiffness, maximum and net loads of infills with different aspect ratios

Fig. 4 shows the stress contour of infilled walls with different aspect ratios when the maximum lateral loads of infills are reached. As shown, the infilled wall experiences a compression along the diagonal direction under the lateral load, however, this diagonal compressive mechanism is gradually altered by increasing the infill aspect ratio. In other words, the assumption of using an equivalent diagonal strut to represent the infilled wall is not suitable for a very large infill aspect ratio.

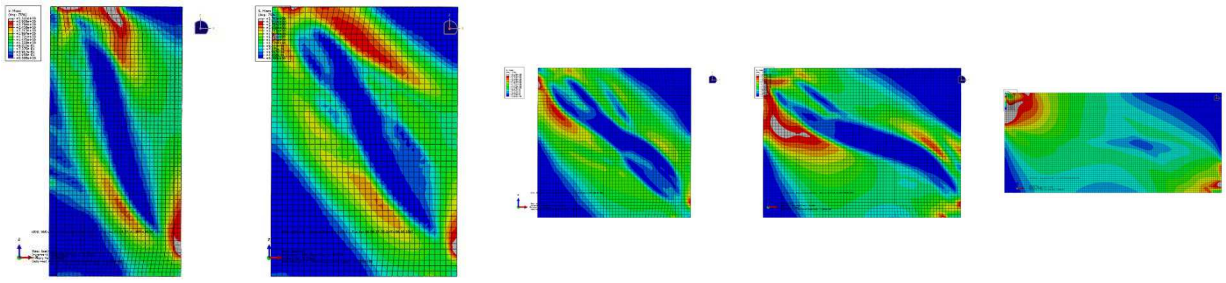

Aspect ratio=0.48 Aspect ratio=0.68 Aspect ratio=1.00 Aspect ratio=1.30 Aspect ratio=2.15

Fig. 4. Stress contour of infills with different aspect ratios

In summary, the infill aspect ratio has a significant influence on the lateral responses of infilled walls including the initial stiffness, maximum lateral load, and net load. Moreover, the diagonal compressive mechanism of infilled walls under the lateral load would be changed by the infill aspect ratio. It is desirable to establish explicit expressions of the key points in the lateral load-displacement relationship of infilled

walls to depict the lateral responses of infilled walls under the entire loading process, and the in-plane behaviour of MIHSFs, therefore, can be estimated.

3.2. Effect of vertical load

In compliance with the design codes of steel framed structures (GB50017 2017), seven different axial compression ratios of the columns are considered to investigate the influence of the vertical load on the lateral responses of infilled walls, which ranges from 0 to 0.6 with an interval of 0.1 and is applied to the FE models as shown in Fig. 1. Two infill aspect ratios of 0.63 and 1.40 are selected as the standard FE models.

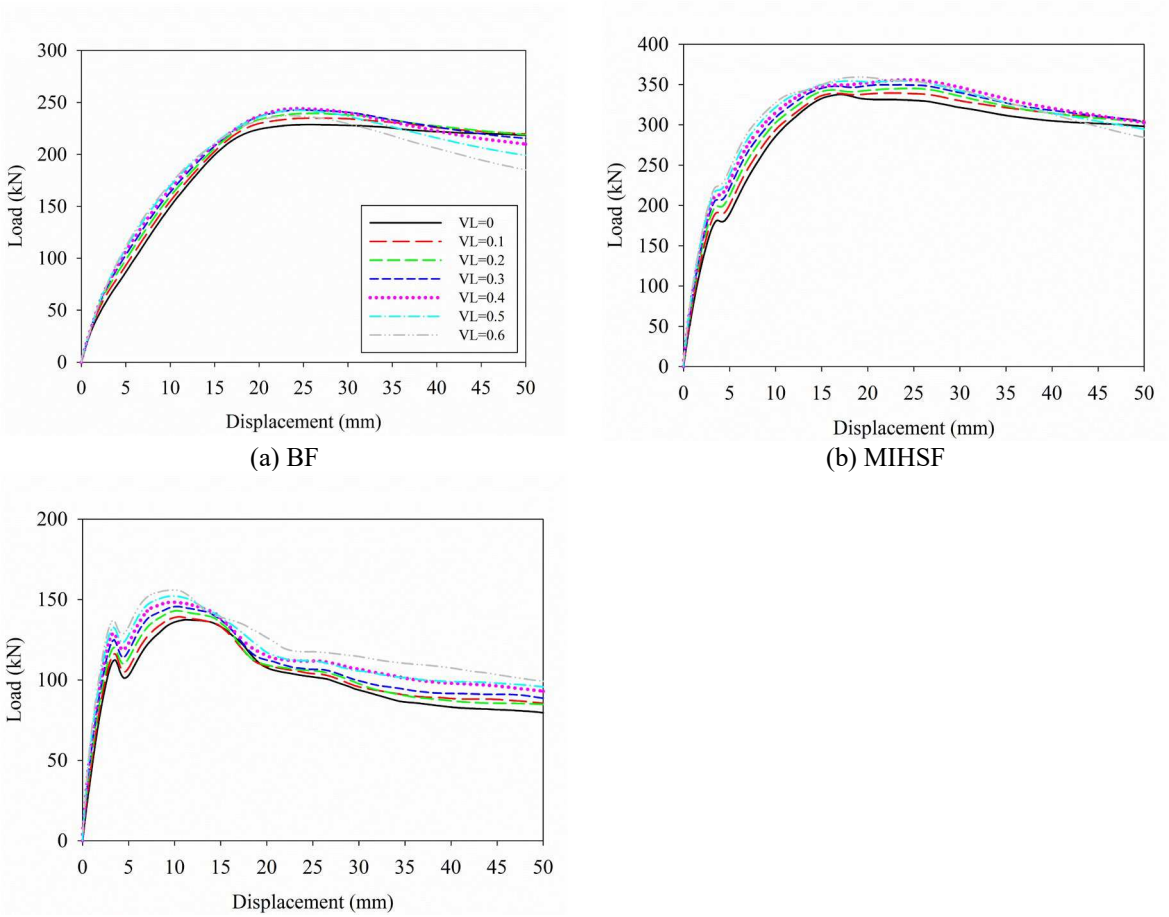

(a) BF (b) MIHSF

(c) Infilled wall

Fig. 5. Lateral load-displacement curves of BF, MIHSF and infilled wall under different vertical load levels

Fig. 5 shows the lateral load-displacement relationships of BF, MIHSF and infilled wall with an aspect ratio of 1.40 when the structures are subjected to different vertical loads. Since the main observations of the effect of the vertical load on the in-plane responses of these two considered infill aspect ratios are the same, only the lateral load-displacement curves of the infill aspect ratio of 1.40 are presented herein for conciseness. As shown in Fig. 5(a), the vertical load almost has no influence on the initial stiffness of BF,

and the lateral load carrying capacity slightly increases with the increase of the applied vertical load while it slightly decreases when the axial compression ratio is larger than 0.4. With increasing the vertical load, the strength degradation in the lateral load-displacement curves of BF becomes more evident, which indicates that the ductility of BFs is decreased by the vertical load. As for MIHSF and the infilled wall, both initial stiffness and lateral load resistance increase with the vertical load as shown in Figs. 5(b) and (c). This is because the vertical load acting on the columns can enhance the corner constraint effect of the surrounding frame on the infilled wall, which leads to the improvement of the stiffness and strength of the infilled wall. Compared to the infilled wall, the increment of the lateral load carrying capacity of MIHSF induced by the vertical load is limited because of the serious damage of the infill. In other words, the lateral displacements corresponding to the maximum loads of MISHF and the infilled wall are different, and the corresponding displacement of the infilled wall is much smaller than that of MIHSF as shown in Figs. 5(b) and (c).

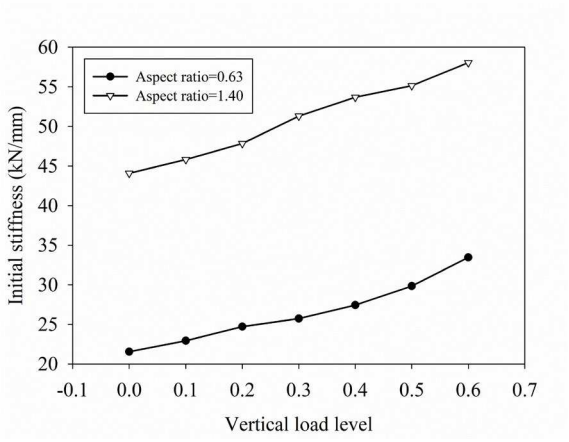

(a) Initial stiffness

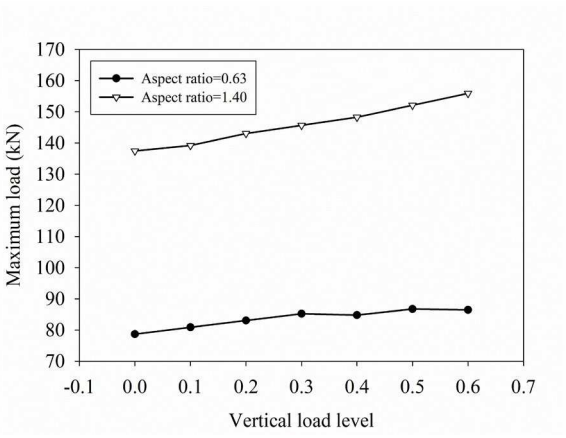

(b) Maximum load

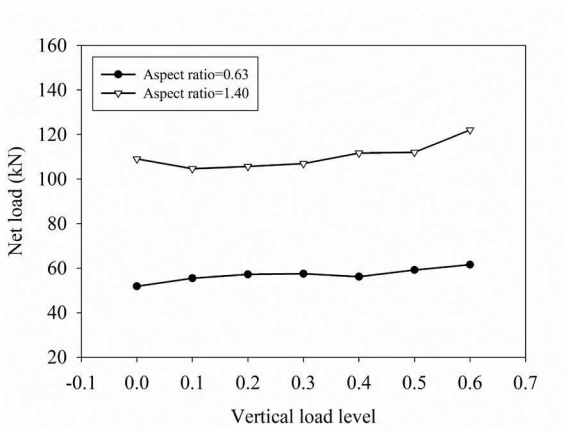

(c) Net load

Fig. 6. Initial stiffness, maximum and net loads of infills under different vertical load levels

Fig. 6 shows the initial stiffness, maximum lateral load, and net load of infilled walls with aspect ratios of 0.63 and 1.40 under varying vertical loads. As shown in Figs. 6(a) and (b), when there is no vertical load

applied to the structure, the initial stiffness and lateral load carrying capacity of the infilled wall with an aspect ratio of 0.63 are 21.6 kN/mm and 78.7 kN, respectively, and they are 33.5 kN/mm and 88.4 kN when the axial compression ratio is 0.6, which increase by 55.1% and 12.3%, respectively; for the infilled wall with an aspect ratio of 1.40, the initial stiffness and lateral load carrying capacity increase by 31.8% and 13.9%, respectively. In general, the initial stiffness and maximum lateral load of infilled walls are affected by the vertical load with different degrees depending on the infill aspect ratio. However, as shown in Fig. 6(c), it seems that the vertical load has a negligible effect on the net load of infilled walls.

3.3. Effect of window opening

To study the influence of window opening on the in-plane responses of masonry infills, the infill aspect ratios of 0.63, 0.90, and 1.40 are taken as the standard FE models. Since the effects are almost the same for these three aspect ratios, only the results of the aspect ratio of 1.40 are presented and discussed in detail in this subsection. Table 3 lists the designed window opening sizes and locations when the infill aspect ratio is 1.40. As tabulated, in total 15 different window openings representing approximately 6-39% of the infill area are investigated. The heights of window openings (h_o) are designed as 600, 900, and 1200 mm, respectively, and the lengths of window openings (l_o) are within the range from 600 to 1800 mm in each opening height. In addition, three different opening locations including central, left-sided, and right-sided are considered for the sizes of 900×600, 1200×900, 1400×1200, and 1800×1200 mm window openings. The eccentricity of window opening (e_c) is measured from the centre of the infill, and the left and right sides are denoted as the negative and positive directions, respectively, for a convenient statement. It is worth noting that the offset value decreases with the increase of the opening length as offsetting the opening far away from the centre of the infill might cause part of the opening outside the infill.

Table 3 Designed window opening sizes and locations in infills with an aspect ratio of 1.40

Model No.	Height h_o (mm)	Length l_o (mm)	Opening area ratio	Eccentricity e_c (mm)
W_1	600	600	0.064	0
W_2		900	0.096	-600, 0, 600
W_3		1200	0.129	0
W_4		1400	0.150	0
W_5		1800	0.193	0
W_6	900	600	0.096	0
W_7		900	0.145	0
W_8		1200	0.193	-400, 0, 400
W_9		1400	0.225	0
W_10		1800	0.289	0
W_11	1200	600	0.129	0
W_12		900	0.193	0
W_13		1200	0.257	0
W_14		1400	0.300	-400, 0, 400
W_15		1800	0.386	-250, 0, 250

Note: W denotes window opening in Table 3.

The effects of window opening sizes on the initial stiffness and strength of infilled walls are shown in Figs. 7-9, respectively. In which, the initial stiffness, maximum lateral load, and net load of infilled walls with window openings are normalized to those of the corresponding solid infill. As anticipated, the stiffness and strength of infilled walls decrease drastically due to the presence of window openings. When the opening area ratio is 38.6%, the stiffness and maximum lateral load of infills are only around 20% of solid infills. Moreover, approximately linear relationships between the ratios of the stiffness and strength of infills with central openings and opening geometries can be found in Figs. 7-9, and explicit formulas can be derived using curve fitting technique to describe their overall relationships, which will be carried out in the following section.

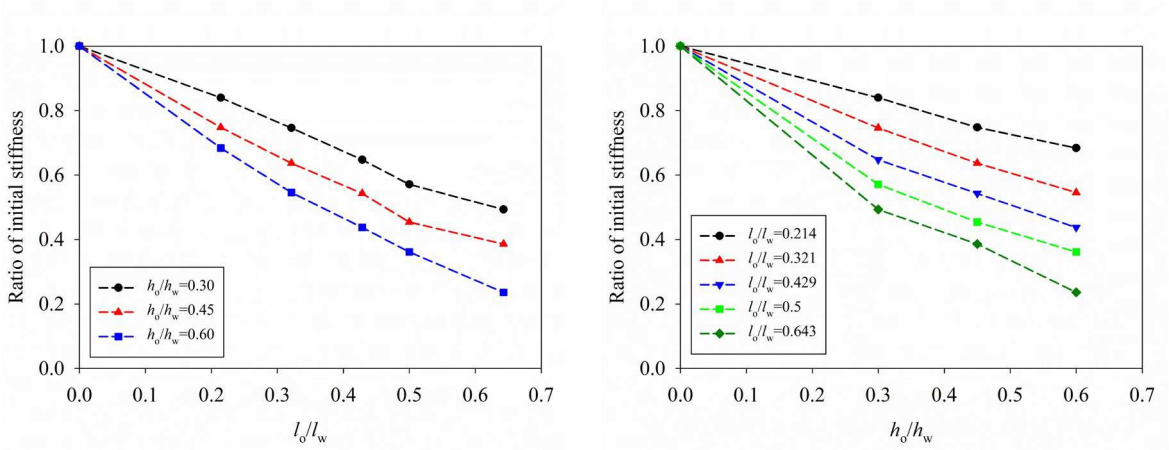

(a) Opening height ratio (b) Opening length ratio

Fig. 7. Ratio of initial stiffness of infills with central window openings

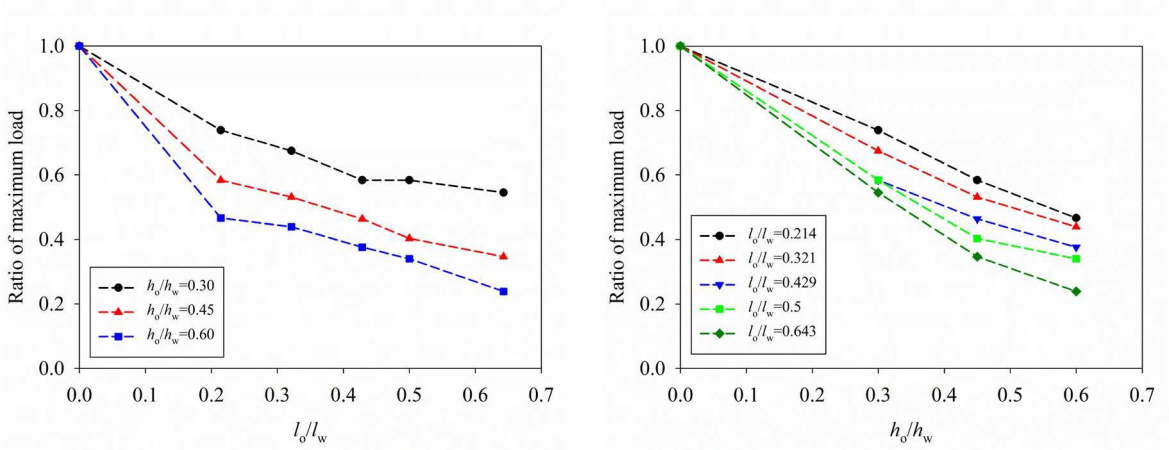

(a) Opening height ratio (b) Opening length ratio

Fig. 8. Ratio of maximum lateral load of infills with central window openings

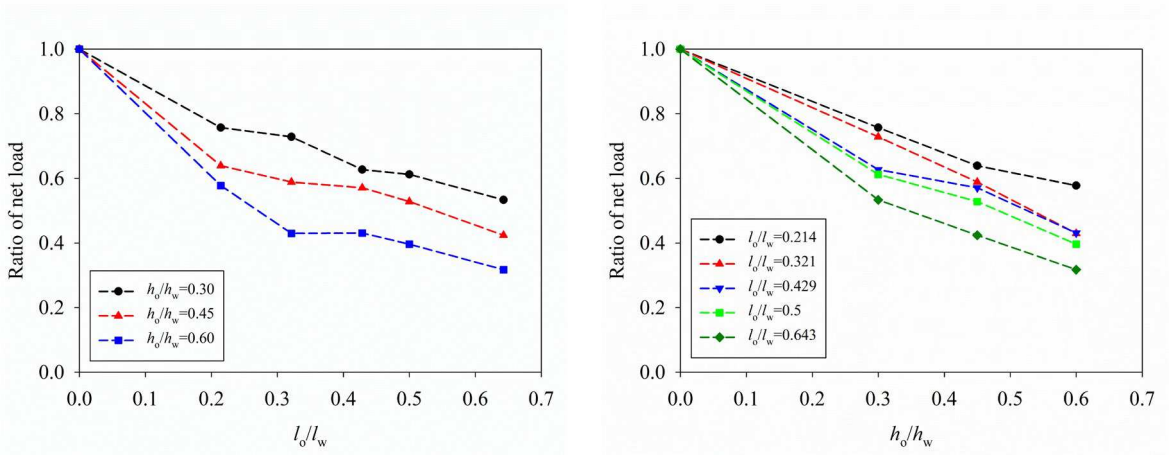

(a) Opening height ratio (b) Opening length ratio

259 Fig. 9. Ratio of net load of infills with central window openings

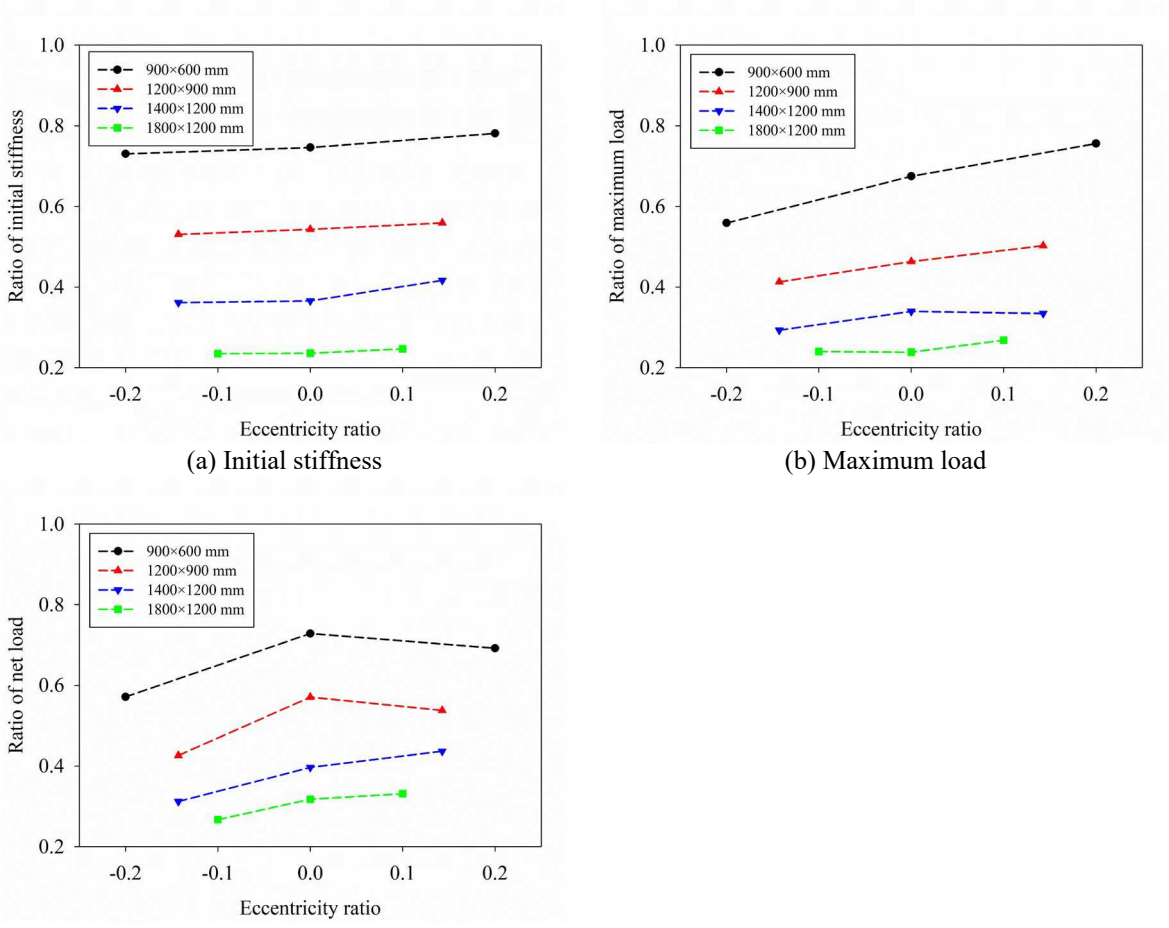

(a) Initial stiffness (b) Maximum load

(c) Net load

260 Fig. 10. Ratios of stiffness and strength of infills with eccentric window openings

261 Fig. 10 shows the variations of the stiffness and strength of perforated infills with the opening eccentricity.
262 Obviously, the initial stiffness and strength of infilled walls are considerably reduced by increasing the
263 window opening area irrespective of the opening location, whereas it affects the reduction rate. When the

window opening shifts from the left to the right side, the reductions on the initial stiffness, maximum lateral load and net load of infilled walls lessen. This can be explained by the stress distribution of the infilled wall with a window opening 900×600 mm shown in Fig. 11. The left and right ones in Figs. 11(a) and (b) are corresponding to the infilled wall starts to crack and reaches its lateral load carrying capacity, respectively. As shown, the window opening is located at a displacement of -600 mm, the left pier is too thin to form a compression strut, while it can still develop a strut leading to an increase in the initial stiffness and strength of the infilled wall when the window opening is at a displacement of +600 mm. In practice, the window opening would be ideally designed at the centre of the infilled wall to resist the lateral load in either direction.

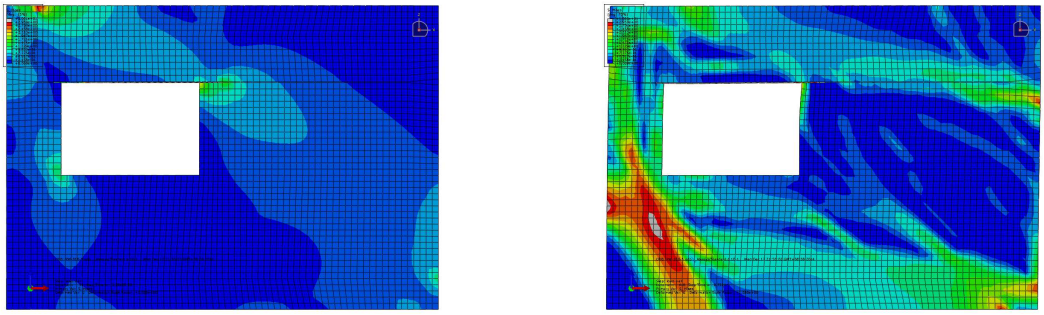

(a) Window opening shifts at a displacement of -600 mm

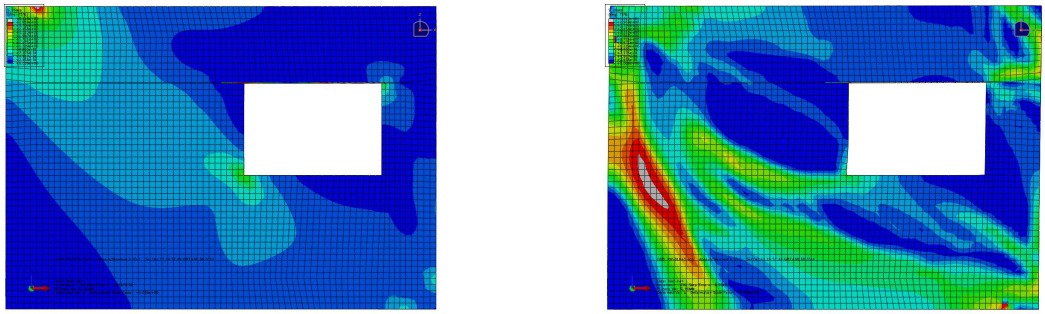

(b) Window opening shifts at a displacement of +600 mm

Fig. 11. Stress contour of infill with a window opening 900×600 mm

3.4. Effect of door opening

Similar to the investigation of the influence of window opening on the in-plane responses of masonry infills performed in Section 3.3, three infill aspect ratios (0.63, 0.90, and 1.40) are assumed as the standard FE models in this subsection to study the effect of door opening. It should be noted that the main observations are almost the same for these three infill aspect ratios, only the results of the aspect ratio of 1.40 are presented and discussed. The designed door opening sizes and locations are given in Table 4.

Table 4 Designed door opening sizes and locations in infills with an aspect ratio of 1.40

Model No.	Height h_o (mm)	Length l_o (mm)	Opening area ratio	Eccentricity e_c (mm)	Eccentricity ratio
D_1	1200	500	0.107	-250, 0, 250	-1/12,0, 1/12
D_2	1200	600	0.129	-500, 0, 500	-1/6, 0, 1/6
D_3	1500	600	0.161	-250, 0, 250	-1/12, 0, 1/12
D_4	1500	700	0.188	-500, 0, 500	-1/6, 0, 1/6
D_5	1700	700	0.213	-250, 0, 250	-1/12, 0, 1/12
D_6	1700	800	0.243	-500, 0, 500	-1/6, 0, 1/6
D_7	1700	1000	0.304	-250, 0, 250	-1/12,0, 1/12

Note: D denotes door opening in Table 4.

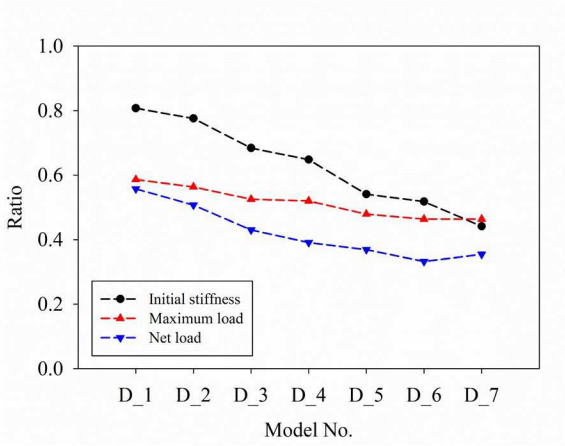

Fig. 12. Ratios of stiffness and strength of infills with central door openings

Fig. 12 shows the initial stiffness, maximum lateral load, and net load of infilled walls with central door openings normalized to those of the corresponding solid infill. As shown, the stiffness and strength of infilled walls significantly degrade with increasing the door opening area especially for the initial stiffness and net load. Moreover, the influences of the door opening eccentricity on the stiffness and strength of infilled walls are presented in Fig. 13. In particular, when the door opening moves from the left to right side, the initial stiffness of infilled walls slightly increases, however, the effects of the eccentricity on the maximum lateral load and net load of infilled walls are not evident compared to the results shown in Fig. 10, and the maximum difference of the strength between the infill with a left- and right-leaned door opening is only about 6%.

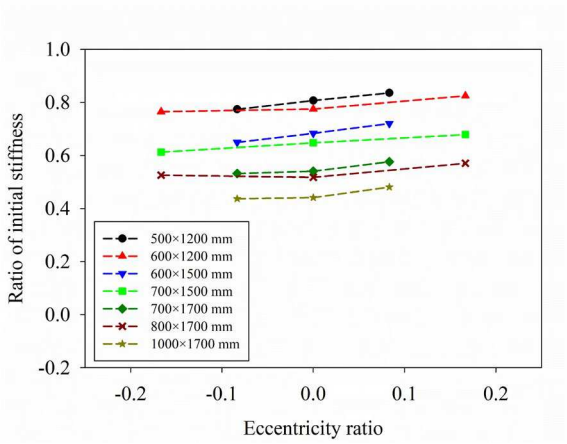

(a) Initial stiffness

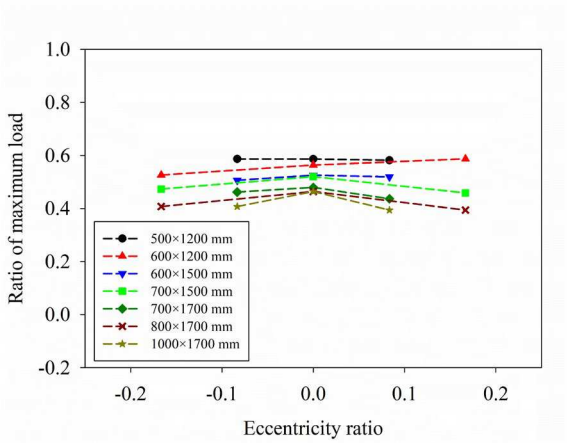

(b) Maximum load

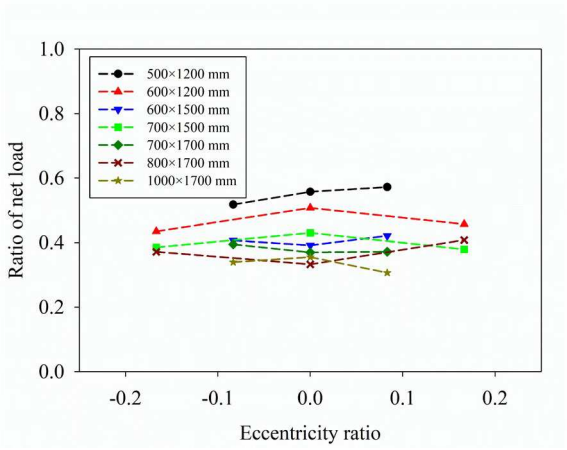

(c) Net load

Fig. 13. Ratios of stiffness and strength of infills with eccentric door openings

4. Force-displacement relationship models

The previous discussion indicates that the in-plane responses of masonry infills cannot be accurately estimated by using an invariant strut width based on the equivalent diagonal strut model, and it is necessary to take the progressive degradation of the infill stiffness and strength into account during the lateral loading, and a force-displacement relationship model for the infill is desired, which should include the influences of the infill aspect ratio, vertical load acting on the surrounding frame, and opening size and location. Prior to proposing a force-displacement relationship for the infill by considering these influential parameters, the commonly adopted model aiming at the appraisal of the in-plane behaviour of the solid infilled frame is briefly introduced.

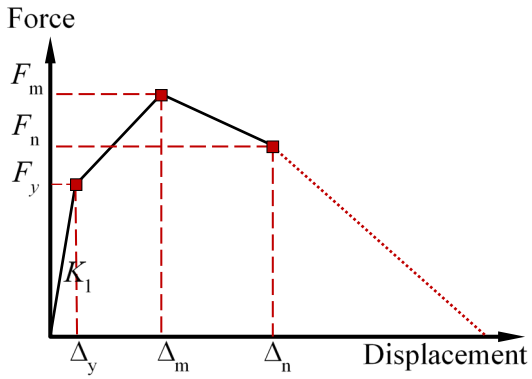

Fig. 14. Force-displacement relationship model for solid infills

Fig. 14 shows a generalized force-displacement relationship model for solid masonry infills, which is composed of three main branches. The first branch corresponds to the linear elastic behaviour of the uncracked infill; the second branch represents the stiffness deterioration of the infill due to the cracking, and the lateral load carried by the infill gradually increases until reaching the load carrying capacity of the infill; and the third branch describes the strength softening of the infill. The key parameters in defining these three branches of the curve are specified as follows.

(1) Infill initial stiffness K_1 (Cavaleri et al. 2005; Papia et al. 2003)

$$K_1 = \frac{E_w w_1 t_w}{d_w} cos^2\theta \tag{1}$$

$$w_1 = k\frac{C}{z}\frac{1}{(\lambda^*)^\beta} d_w \tag{2}$$

$$C = 0.249 - 0.0116\nu + 0.567\nu^2 \tag{3a}$$

$$\beta = 0.146 + 0.0073\nu + 0.126\nu^2 \tag{3b}$$

$$k = 1 + (18\lambda^* + 200)\varepsilon_v \tag{4a}$$

$$\varepsilon_v = \frac{N}{E_f A_c} \tag{4b}$$

$$\lambda^* = \frac{E_w t_w h_f}{E_f A_c}\left(\frac{h_f^2}{l_f^2} + \frac{1}{4}\frac{A_c}{A_b}\frac{l_f}{h_f}\right) \tag{4c}$$

In which, E_w is the Young's modulus of the masonry material; t_w and d_w are the thickness and diagonal length of the infill, respectively; θ is the inclined angle of the infill diagonal; w_1 is the strut width corresponding to the linear elastic behaviour of the infill and can be calculated by Eq. (2) including the effects of Poisson ratio of the masonry material, infill aspect ratio, and vertical load. In particular, the influence of Poisson ratio of the masonry material on the strut width is explicitly quantified by two

parameters C and β as given by Eq. (3), and ν is the Poisson ratio. Parameter k denotes the effect of vertical load and is estimated by Eq. (4). In Eq. (4), N is the vertical load; E_f is the Young's modulus of the confining frame; A_c and A_b are the cross-sectional areas of the frame columns and beam; h_f and l_f are the height and length of the frame. It should be noted that parameter z is used to consider the influence of infill aspect ratio, however, only two different infill aspect ratios were investigated in developing the strut width in Papia et al. (2003), and the values of the parameter z were suggested as 1 and 1.125 when the infill aspect ratios were 1 and 1.5, respectively.

(2) Yielding force F_y (Uva et al. 2012b)

$$F_y = f_t t_w l_w \tag{5}$$

where f_t is the tensile strength of the infill and can be obtained by the diagonal compression test, and l_w is the length of the infill.

(3) Maximum force F_m

The lateral load carrying capacity of the solid infill was simply assumed as 1.3 times of the yielding force in Uva et al. (2012b), and this coefficient will be further validated by taking the effects of infill aspect ratio, vertical load, and opening into account in the present study.

(4) Displacement Δ_m corresponding to the maximum force

$$\Delta_m = \frac{\varepsilon_m d_w}{\cos\theta} \tag{6}$$

where ε_m is the peak compression strain of the masonry material, and the value of ε_m is approximately 0.25%.

(5) Net force F_n

As mentioned above, the net force of the infill is defined as the contribution of the infill to the ultimate load of the infilled frame system, which is given by

$$F_n = f_c t_w w_m \cos\theta \tag{7}$$

In which, f_c is the compressive strength along the diagonal direction of the infill (El-Dakhakhni et al. 2003), and w_m is the strut width corresponding to the maximum load carried by the infilled frame, and can be calculated by (Mainstone 1971)

$$w_m = 0.175\left(\lambda h_f\right)^{-0.4} d_w \tag{8a}$$

$$\lambda = \sqrt[4]{\frac{E_w t_w \sin 2\theta}{4E_f I_c h_w}} \tag{8b}$$

where λ is the stiffness ratio between the infill and bounding frame, and I_c is the moment of inertia of the frame column.

(6) Displacement Δ_n corresponding to the net force

The statistical analysis of the previous experimental results revealed that the drift ratio corresponding to the lateral load resistance of masonry infilled steel frames was normally about 1.0%, which is adopted in the present study for simplicity. Therefore, the displacement corresponding to the net force of the infill is expressed by

$$\Delta_n = 0.01 h_f \tag{9}$$

Although the generalized force-displacement relationship of masonry infills shown in Fig. 14 were often used in the structural response estimations of infilled frames, the influences of infill aspect ratio, vertical load, and opening size and location were not comprehensively investigated, which will be studied in the rest of this section by using a curve fitting method to analyse the numerical results obtained in Section 3.

4.1. Solid infills

As discussed in Sections 3.1 and 3.2, the initial stiffness and maximum lateral load of the solid infill are significantly influenced by both infill aspect ratio and vertical load, however, the net load of the solid infill is only affected by the infill aspect ratio. Therefore, the calculations of the stiffness and strength of the solid infill in the above model (see Fig. 14) are updated by considering these two influential parameters.

By using the results of the initial stiffness of the solid infill under different infill aspect ratios presented in Section 3.1, the values of the parameter z in Eq. (2) can be determined, and they are shown in Fig. 15. As shown, the values of the parameter z vary around 1.0 when the aspect ratio is smaller than 1.0, however, when it is larger than 1.0, the values of the parameter z increase with increasing the infill aspect ratio. This is because Eq. (2) was proposed based on the stiffness equivalence between the diagonal strut model and actual infilled steel frame (Papia et al. 2003), but the infill cannot be simply assumed as an equivalent diagonal strut with the increased infill aspect ratio as demonstrated in Section 3.1, which is a discrepancy between the simplified model and practical infilled frame. A fitting formula is developed to calculate the parameter z under the investigated infill aspect ratios in the present study, which is given by

$$z = \begin{cases} 1 & 0.48 \le \dfrac{l_w}{h_w} \le 1 \\ 1 + 0.35\left(\dfrac{l_w}{h_w} - 1\right) & 1 < \dfrac{l_w}{h_w} \le 2.15 \end{cases} \quad (10)$$

With regards to the effect of the vertical load, the initial stiffness of the solid infill linearly increases with the vertical load as shown in Fig. 6(a), and Eq. 4(a) proposed by Papia et al. (2003) is still capable of estimating the effect of the vertical load on the initial stiffness of the solid infill.

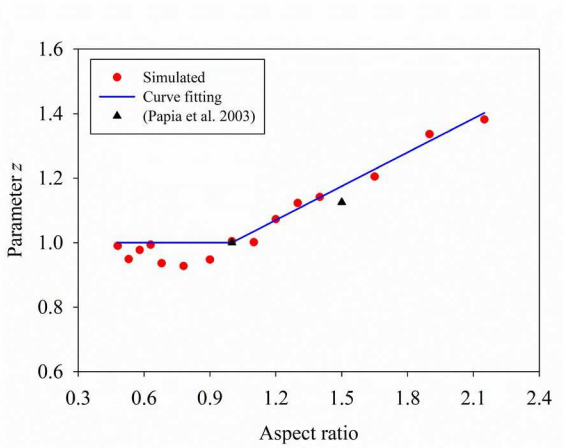

Fig. 15. Values of parameter z in Eq. (2) under varying infill aspect ratios

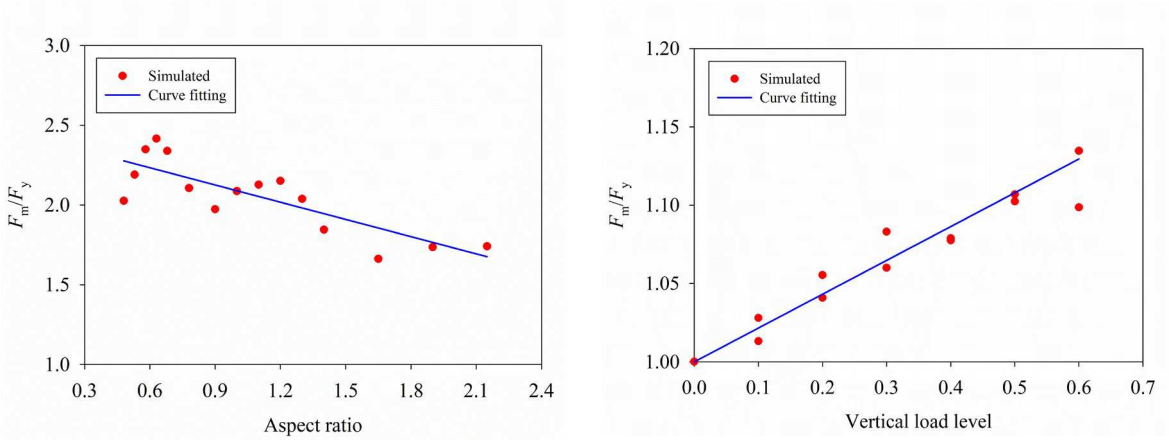

(a) Aspect ratio (b) Vertical load

Fig. 16. Effects of aspect ratio and vertical load on the maximum lateral load of solid infills

Fig. 16 shows the effects of aspect ratio and vertical load on the lateral load carrying capacity of solid infills. In this figure, the maximum lateral load is normalized to the yielding load of the respective solid infill, and the latter is calculated by Eq. (5). As shown, the overall trend of the ratio between the maximum lateral load and yielding load decreases with the increase of the infill aspect ratio, while it increases with the applied vertical load on the frame columns. Compared to the effect of vertical load, the variability of the effect of the infill aspect ratio on the maximum lateral load of the solid infill is much larger, which is

consistent with the results shown in Figs. 3(b) and 6(b). The relationship between the maximum lateral load and yielding load of the solid infill can be described by using a fitting formula with the consideration of the effects of the infill aspect ratio and vertical load, which is expressed by

$$F_m = \left(2.45 - 0.36\frac{l_w}{h_w}\right)(1 + 0.21\mu)F_y \tag{11}$$

where μ is the axial compression ratio.

Furthermore, the net load of the solid infill is only influenced by the infill aspect ratio, and the vertical load has a marginal effect. The simulated and calculated (by Eq. (7)) net loads of solid infills with different aspect ratios are compared in Fig. 17. As shown, the net loads of solid infills calculated by Eq. (7) are in well agreement with the simulated results when the aspect ratio is smaller than 1.50, however, the net loads of solid infills are overestimated by Eq. (7) when the infill aspect ratio is larger than 1.50. Thus, a modified factor is proposed in the present study to predict the net load of the solid infill more accurately under varying infill aspect ratios, which is given by

$$F_n = \alpha f_c t_w w_m \cos\theta \tag{12}$$

$$\alpha = \begin{cases} 1 & 0.48 \le \dfrac{l_w}{h_w} \le 1.5 \\ 1 - \dfrac{4}{7}\left(\dfrac{l_w}{h_w} - 1.5\right) & 1.5 < \dfrac{l_w}{h_w} \le 2.15 \end{cases} \tag{13}$$

where α is the modified factor.

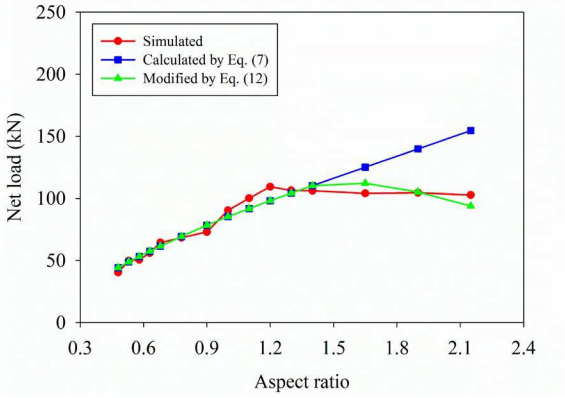

Fig. 17. Net loads of solid infills with different aspect ratios

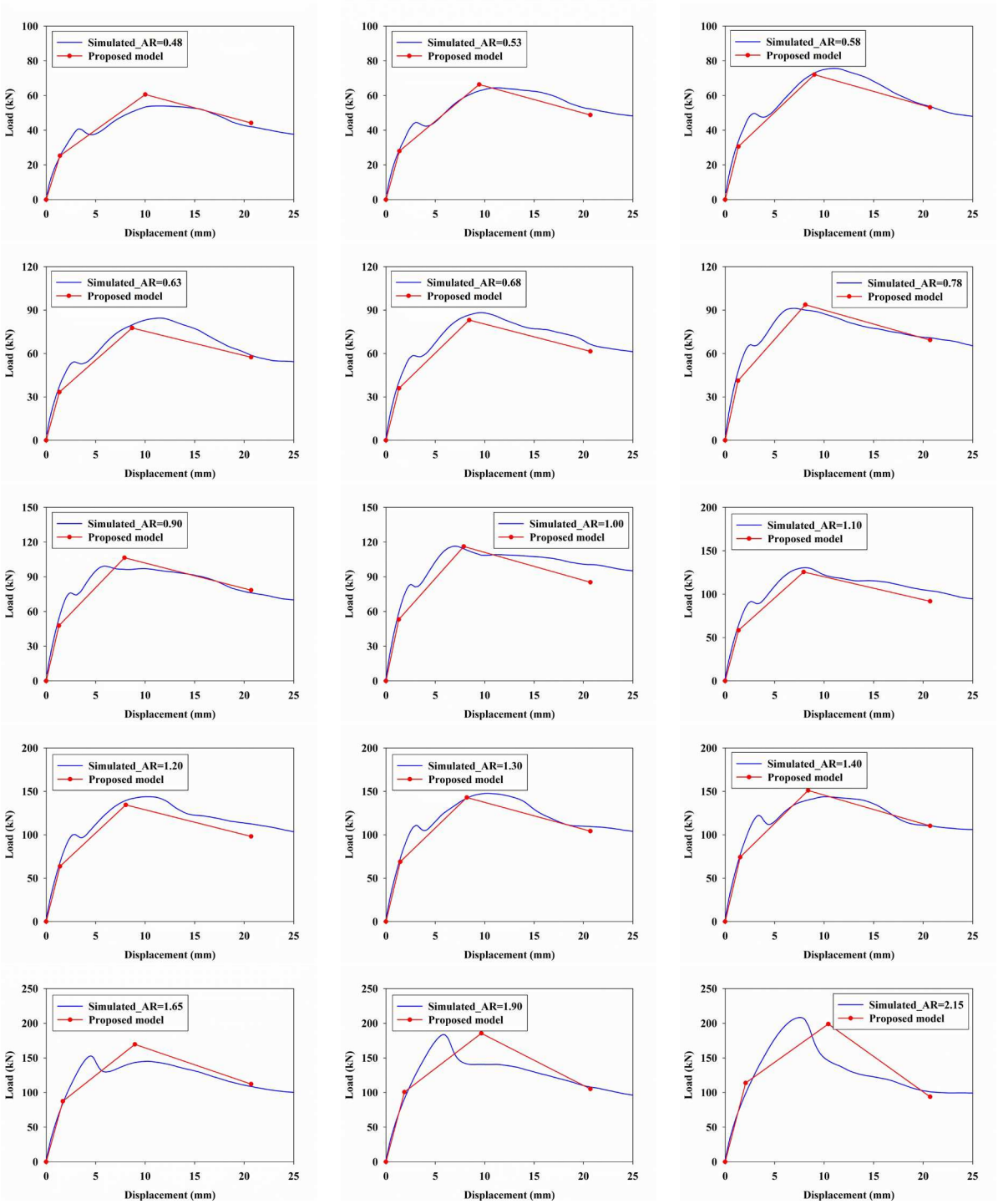

Fig. 18. Comparison of force-displacement curves of solid infills with different aspect ratios

Based on the above modifications, the critical points on the force-displacement curve of the solid infill can be determined by taking the influences of infill aspect ratio and vertical load into account. To validate the accuracy of the proposed formulas, the simulated force-displacement curves of solid infills under the considered aspect ratios and vertical load levels are compared with those estimated by the above model in

Figs. 18 and 19, respectively. As can be seen, the proposed force-displacement curves of solid infills under different aspect ratios and vertical loads match well with the simulated results. However, it needs to point out that a large difference of the displacement corresponding to the lateral load carrying capacity of the infill between the proposed model and simulated results is observed especially when a large infill aspect ratio is adopted. This is because the equivalent strut model is not suitable for a large infill aspect ratio as discussed above, which might lead to a slightly larger error. General speaking, the initial stiffness, maximum lateral load, and net load and their corresponding displacements can be accurately evaluated by the proposed model.

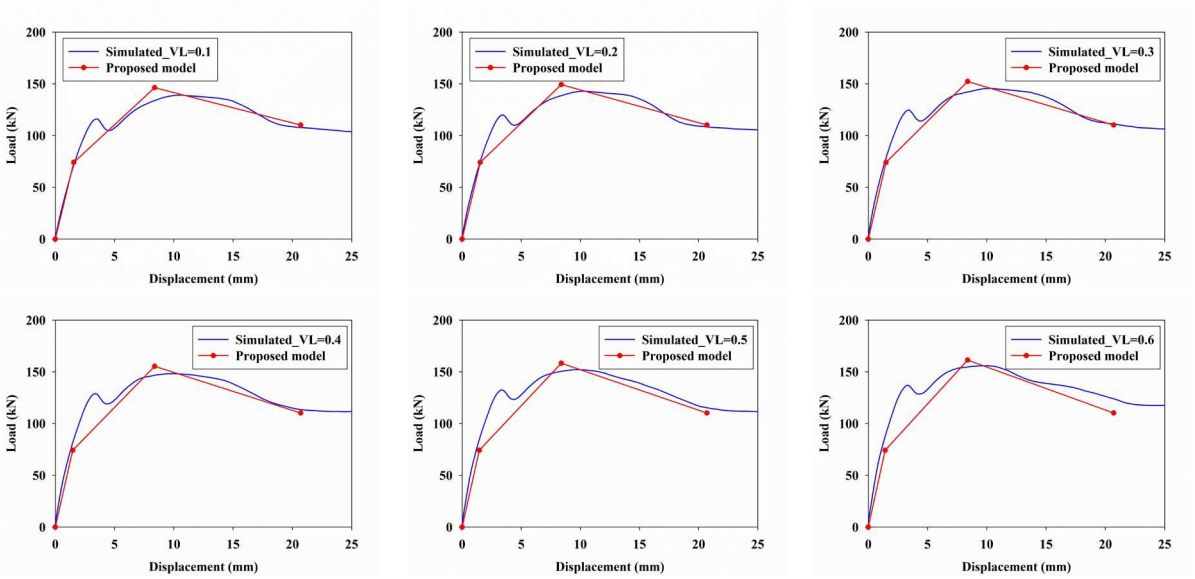

Fig. 19. Comparison of force-displacement curves of solid infill under different vertical loads

4.2. Infills with window and door openings

The results in Sections 3.3 and 3.4 indicate that the opening size and location are two main factors influencing the stiffness and strength of perforated infills. To be specific, the initial stiffness of infills with openings is influenced by both opening size and location, however, the opening location has a negligible effect on the maximum lateral load and net load of perforated infills. The present study combines the effects of opening size and location in a generalized reduction factor of the stiffness and strength of perforated infills, which is expressed by

$$R = 1 - f\left(\frac{l_o}{l_w}, \frac{h_o}{h_w}\right) g\left(\frac{e_c}{l_w}\right) \tag{14}$$

Moreover, it should be noted that the calculation of the yielding force of infills with openings is correspondingly modified to

$$F_y = f_t t_w (l_w - l_o) \tag{15}$$

Through nonlinear regression analysis on the numerical results of infills with window openings, the expressions of $f\left(\frac{l_o}{l_w}, \frac{h_o}{h_w}\right)$ and $g\left(\frac{e_c}{l_w}\right)$ for the ratios of the stiffness and strength between the perforated and solid infills are determined as follows.

For the initial stiffness of infills with window openings:

$$f\left(\frac{l_o}{l_w}, \frac{h_o}{h_w}\right) = 0.248\frac{l_o}{l_w} + 0.266\frac{h_o}{h_w} + 1.202\frac{l_o}{l_w}\frac{h_o}{h_w} \tag{16a}$$

$$g\left(\frac{e_c}{l_w}\right) = 1 + 0.664\frac{e_c}{l_w} \tag{16b}$$

For the maximum lateral load (Eq. (17)) and net load (Eq. (18)) of infills with window openings:

$$f\left(\frac{l_o}{l_w}, \frac{h_o}{h_w}\right) = -1.180\frac{l_o}{l_w} + 0.757\frac{h_o}{h_w} + 1.588\frac{l_o}{l_w}\frac{h_o}{h_w} \tag{17}$$

$$f\left(\frac{l_o}{l_w}, \frac{h_o}{h_w}\right) = 0.222\frac{l_o}{l_w} + 0.290\frac{h_o}{h_w} + 0.915\frac{l_o}{l_w}\frac{h_o}{h_w} \tag{18}$$

Taking the infill with an aspect ratio of 1.40 as an example, the simulated and calculated results on the initial stiffness, maximum lateral load, and net load of the infill with various window opening sizes are compared in Fig. 20. In this figure, the results from the FE analysis are denoted in dots, and the results calculated by using the above curve-fitted equations are depicted by dashed lines. As shown, a good correlation (R^2>0.97) between the simulated and calculated results for both stiffness and strength is achieved.

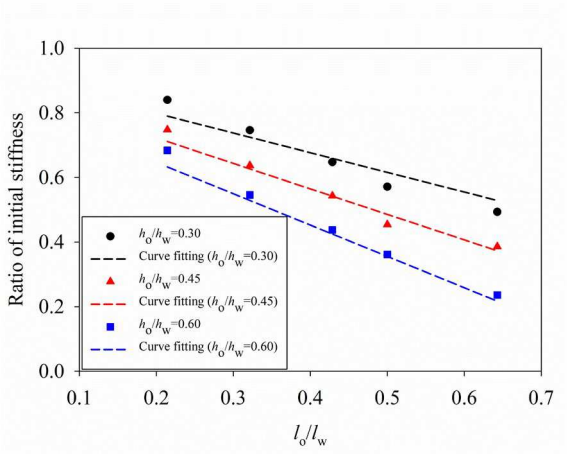

(a) Initial stiffness

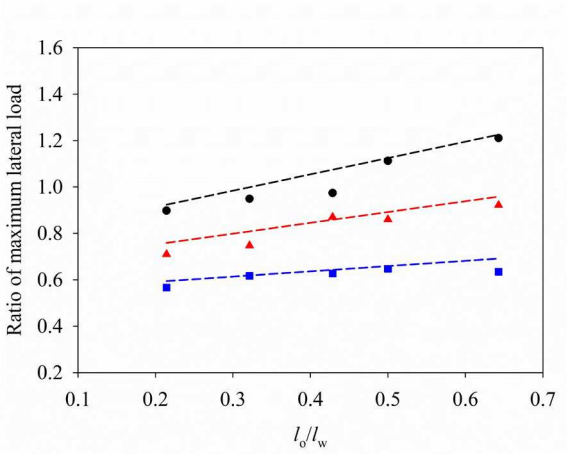

(b) Maximum lateral load

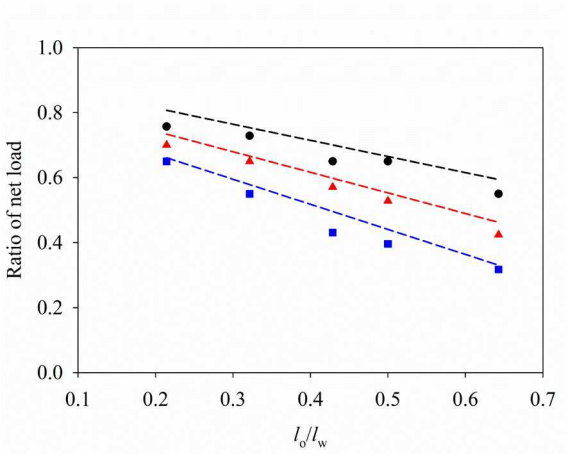

(c) Net load

Fig. 20. Simulated and calculated ratios of stiffness and strength of infills with window openings

For the infills with door openings, the same regression analysis can be performed, and the functions to consider the influences of door opening size and location are derived as follows.

For the initial stiffness of infills with door openings:

$$f\left(\frac{l_o}{l_w},\frac{h_o}{h_w}\right) = -2.207\frac{l_o}{l_w} + 0.346\frac{h_o}{h_w} + 3.546\frac{l_o}{l_w}\frac{h_o}{h_w} \tag{19a}$$

$$g\left(\frac{e_c}{l_w}\right) = 1 + 0.850\frac{e_c}{l_w} \tag{19b}$$

For the maximum lateral load (Eq. (20)) and net load (Eq. (21)) of infills with door openings:

$$f\left(\frac{l_o}{l_w},\frac{h_o}{h_w}\right) = -2.123\frac{l_o}{l_w} + 0.564\frac{h_o}{h_w} + 2.374\frac{l_o}{l_w}\frac{h_o}{h_w} \tag{20}$$

$$f\left(\frac{l_o}{l_w},\frac{h_o}{h_w}\right) = -0.180\frac{l_o}{l_w} + 0.672\frac{h_o}{h_w} + 0.556\frac{l_o}{l_w}\frac{h_o}{h_w} \tag{21}$$

The force-displacement curves of the infill with an aspect ratio of 1.40 and designed window and door opening tabulated in Tables 3 and 4 are compared with the modified force-displacement relationship model for infills with openings, which are given in Figs. 21 and 22. For conciseness, not all the force-displacement curves of the infill with designed opening sizes and locations are presented, and only the results of several representative window and door openings are compared. As shown in Figs. 21 and 22, the proposed model can accurately predict the in-plane behaviour of the infill with window and door openings, however, the displacement corresponding to the maximum lateral load of the infill with door openings is relatively overestimated by the proposed model.

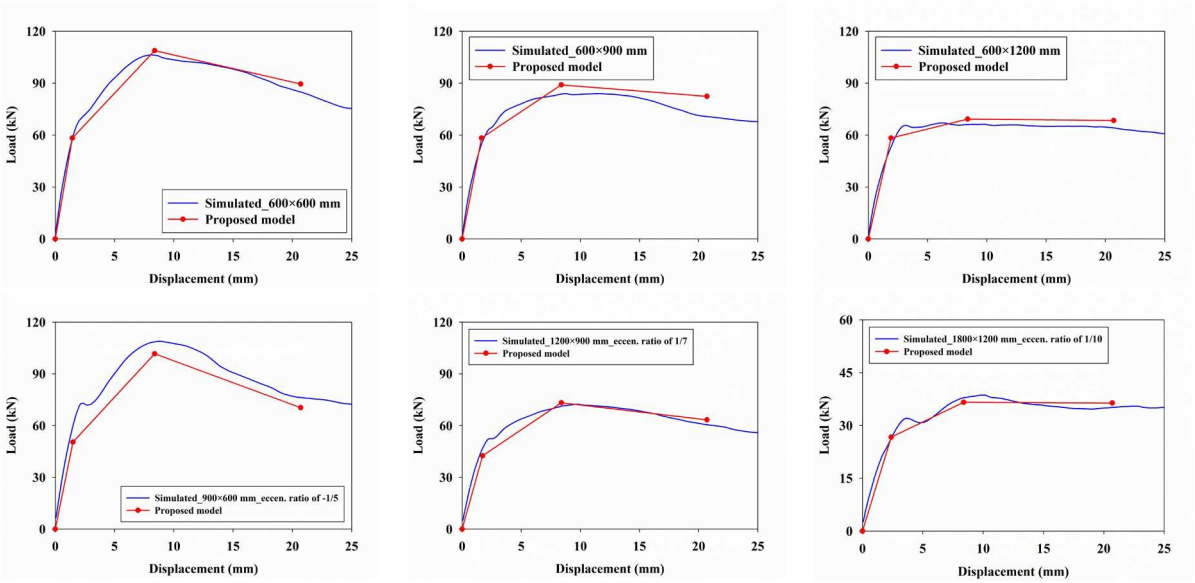

Fig. 21. Comparison of force-displacement curves of infills with window openings

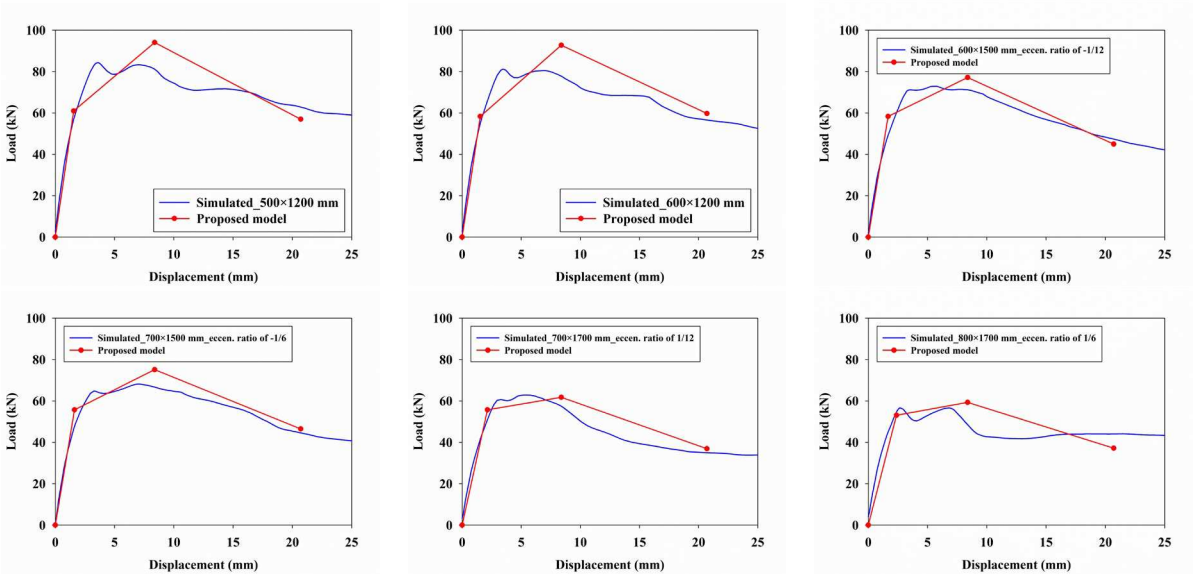

Fig. 22. Comparison of force-displacement curves of infills with door openings

4.3. Validation with experimental tests

To further validate the efficacy of the developed force-displacement relationship model for masonry infills, the experimental tests on both solid infills and infills with openings carried out by Tasnimi and Mohebkhah (2011) are selected for comparison. Table 5 summarizes the geometrical configurations and material properties of the test specimens reported in Tasnimi and Mohebkhah (2011), which will be used to determine the force-displacement curves of infills. Interested readers can find more details of the tests in Tasnimi and Mohebkhah (2011). Fig. 23 compares the calculated force-displacement curves of the solid infills and infills with window and door openings with the test results. As shown, both stiffness and strength

of infills decrease with increasing the opening area, and the analytical results are in well agreement with the experimental results except that a relatively noticeable difference is observed in Fig. 23(c), because the backbone curves of Specimen 3 were different in the push and pull directions (Tasnimi and Mohebkhah 2011), and their average results are shown in Fig. 23. In general, it confirms that the proposed equations can be used to predict the initial stiffness, lateral load carrying capacity, and net load of infills without and with openings.

Table 5 Geometries and material properties of infills (Tasnimi and Mohebkhah 2011)

Specimen	Height h_w (mm)	Length l_w (mm)	Opening height h_o (mm)	Opening length l_o (mm)	Compressive strength of masonry (MPa)	Elastic modulus of masonry (MPa)	Compressive strength of mortar (MPa)	Shear bond strength (MPa)
1	1800	2260	-	-	7.4	7448		
2	1800	2260	500	500	7.4	7448		
3	1800	2260	800	700	7.0	6852	10.1	0.48
4	1800	2260	600	1200	7.0	6852		
5	1800	2260	1450	700	8.5	9169		

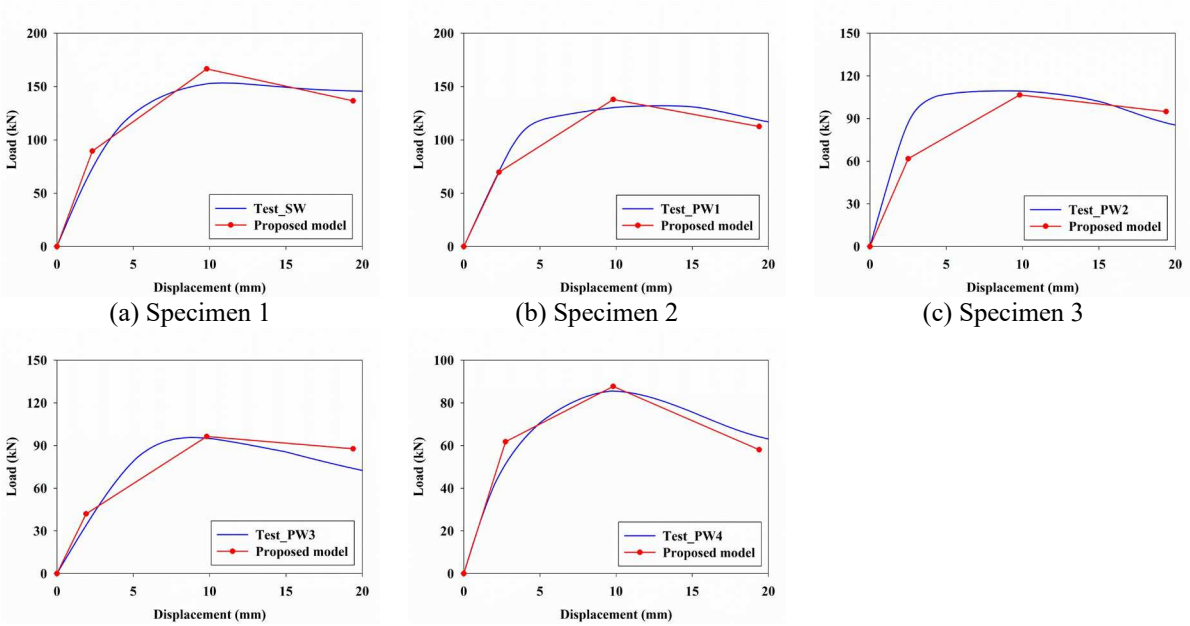

(a) Specimen 1 (b) Specimen 2 (c) Specimen 3

(d) Specimen 4 (e) Specimen 5

Fig. 23. Comparison of force-displacement curves of infills between the proposed model and tests

5. Conclusions

The influences of infill aspect ratio, vertical load acting on the surrounding frames, and opening on the in-plane behaviour of MIHSFs are systematically investigated in the present study. A generalized force-displacement relationship model of infills is proposed by taking the above influential parameters into

account, and the critical parameters in the proposed model are explicitly expressed based on regression analyses of numerical results. Moreover, the credit of the proposed model is examined with numerical and experimental test results. The main findings are summarized as follows.

(1) Both initial stiffness and maximum load of infills are considerably increased with increasing the infill aspect ratio and vertical load on the confining frame, while the net load of infills is not changed with the infill aspect ratio when it is above a certain range, and the vertical load has a negligible effect on the infill net load. In addition, it is noteworthy that the equivalent diagonal strut assumption is debatable when the infill has a large aspect ratio.

(2) The reductions of infill initial stiffness and strength of induced by openings are heavily dependent on the opening area as well as the opening location especially when the window openings shift toward the loaded side, while this effect is not very evident on the strength of infills with door openings. In general, the reductions on the stiffness and strength have an approximately linear relationship with the opening length ratio, height ratio, and eccentricity ratio.

(3) The force-displacement curves of infills without and with openings predicted by the proposed model are in well agreement with the simulated and test results, which indicates that the modified force-displacement displacement relationship model for solid and perforated infills in the present study can be used for structural designs and analyses of infilled steel frames.

Furthermore, it is noteworthy that the force-displacement relationships of infills without and with openings are established on a basis of hinged steel frames, and their applications in RC structures need to be further investigated in future studies.

Acknowledgements

The financial support from the Research Project of Science and Technology Commission of Shanghai Municipality (No. 19DZ1202400) for carrying out this research is highly appreciated.

Compliance with ethical standards

Conflict of interest: The authors declare that they have no conflict of interest.

References

Alwashali H, Sen D, Jin K, Maeda M (2019) Experimental investigation of influences of several parameters on seismic capacity of masonry infilled reinforced concrete frame. Eng Struct 189:11-24

Asteris PG, Antoniou S, Sophianopoulos DS, Chrysostomou CZ (2011) Mathematical macromodeling of infilled frames: state of the art. J Struct Eng 137:1508-1517
Asteris PG, Cotsovos DM, Chrysostomou C, Mohebkhah A, Al-Chaar G (2013) Mathematical micromodeling of infilled frames: state of the art. Eng Struct 56:1905-1921
Benavent-Climent A, Ramírez-Márquez A, Pujol S (2018) Seismic strengthening of low-rise reinforced concrete frame structures with masonry infill walls: shaking-table test. Eng Struct 165:142-151
Campione G, Cavaleri L, Macaluso G, Amato G, Di Trapani F (2015) Evaluation of infilled frames: an updated in-plane-stiffness macro-model considering the effects of vertical loads. Bull Earthq Eng 13:2265-2281
Cavaleri L, Di Trapani F (2014) Cyclic response of masonry infilled RC frames: Experimental results and simplified modeling. Soil Dyn Earthq Eng 65:224-242
Cavaleri L, Di Trapani F, Asteris PG, Sarhosis V (2017) Influence of column shear failure on pushover based assessment of masonry infilled reinforced concrete framed structures: A case study. Soil Dyn Earthq Eng 100:98-112
Cavaleri L, Fossetti M, Papia M (2005) Infilled frames developments in the evaluation of cyclic behaviour under lateral loads. Struct Eng Mech 21:469-494
Chen X, Liu Y (2015) Numerical study of in-plane behaviour and strength of concrete masonry infills with openings. Eng Struct 82:226-235
Chen X, Liu Y (2016) A finite element study of the effect of vertical loading on the in-plane behavior of concrete masonry infills bounded by steel frames. Eng Struct 117:118-129
Di Trapani F, Bolis V, Basone F, Preti M (2020) Seismic reliability and loss assessment of RC frame structures with traditional and innovative masonry infills. Eng Struct 208:110306
Di Trapani F, Macaluso G, Cavaleri L, Papia M (2015) Masonry infills and RC frames interaction: literature overview and state of the art of macromodeling approach. Eur J Environ Civil Eng 19:1059-1095
Dolšek M, Fajfar P (2008) The effect of masonry infills on the seismic response of a four-storey reinforced concrete frame-a deterministic assessment. Eng Struct 30:1991-2001
El-Dakhakhni WW, Elgaaly M, Hamid AA (2003) Three-strut model for concrete masonry-infilled steel frames. J Struct Eng 129:177-185
Gentile R, Pampanin S, Raffaele D, Uva G (2019) Non-linear analysis of RC masonry-infilled frames using the SLaMA method: part 1-mechanical interpretation of the infill/frame interaction and formulation of the procedure. Bull Earthq Eng 17:3283-3304
Gu X, Wang L, Zhang W, Cui W (2018) Cyclic behaviour of hinged steel frames enhanced by masonry columns and/or infill walls with/without CFRP. Struct Infrastruct Eng 14:1470-1485
Humayun Basha S, Surendran S, Kaushik HB (2020) Empirical models for lateral stiffness and strength of masonry-infilled rc frames considering the influence of Openings. J Struct Eng 146:04020021
Kakaletsis D, Karayannis C (2008) Influence of masonry strength and openings on infilled R/C frames under cycling loading. J Earthq Eng 12:197-221
Klingner RE, Bertero V (1978) Earthquake resistance of infilled frames. J Struct Div 104:973–989
Li C, Hao H, Bi K (2019) Seismic performance of precast concrete-filled circular tube segmental column under biaxial lateral cyclic loadings. Bull Earthq Eng 17:271-296
Liauw T-C, Kwan K-H (1984) Nonlinear behaviour of non-integral infilled frames. Comput Struct 18:551-560
Liu Y, Manesh P (2013) Concrete masonry infilled steel frames subjected to combined in-plane lateral and axial loading-An experimental study. Eng Struct 52:331-339
Mainstone RJ (1971) On the stiffness and strengths of infilled frame. Proc Inst Civil Eng Supplement IV:57-90
Markulak D, Radić I, Sigmund V (2013) Cyclic testing of single bay steel frames with various types of masonry infill. Eng Struct 51:267-277
Mohammadi M, Emami SMM (2019) Multi-bay and pinned connection steel infilled frames: an experimental and numerical study. Eng Struct 188:43-59
Mohammadi M, Nikfar F (2013) Strength and stiffness of masonry-infilled frames with central openings based on experimental results. J Struct Eng 139:974-984
Ministry of Housing and Urban-Rural Development of the People's Republic of China (MOHURD) (2010) Code for design of concrete structures-GB50010. Architecture and Building Press, Beijing (*in Chinese*)
Ministry of Housing and Urban-Rural Development of the People's Republic of China (MOHURD) (2011) Code for design of masonry structures-GB50003. Architecture and Building Press, Beijing (*in Chinese*)
Ministry of Housing and Urban-Rural Development of the People's Republic of China (MOHURD) (2017) Code for design of steel structures-GB50017. Architecture and Building Press, Beijing (*in Chinese*)

552 Morandi P, Hak S, Magenes G (2018) Performance-based interpretation of in-plane cyclic tests on RC frames with
553 strong masonry infills. Eng Struct 156:503-521
554 Papia M, Cavaleri L, Fossetti M (2003) Infilled frames developments in the evaluation of the stiffening effect of infills.
555 Struct Eng Mech 16:675-693
556 Perrone D, Leone M, Aiello MA (2017) Non-linear behaviour of masonry infilled RC frames: Influence of masonry
557 mechanical properties. Eng Struct 150:875-891
558 Polyakov S (1960) On the interaction between masonry filler walls and enclosing frame when loaded in the plane of
559 the wall. Translation in Earthquake Engineering. Earthquake Engineering Research Institute (EERI), San
560 Francisco, California, pp 36-42
561 Shing PB, Mehrabi AB (2002) Behaviour and analysis of masonry-infilled frames. Prog Struct Eng Mater 4:320-331
562 Tasnimi A, Mohebkhah A (2011) Investigation on the behavior of brick-infilled steel frames with openings,
563 experimental and analytical approaches. Eng Struct 33:968-980
564 Uva G, Porco F, Fiore A (2012a) Appraisal of masonry infill walls effect in the seismic response of RC framed
565 buildings: A case study. Eng Struct 34:514-526
566 Uva G, Raffaele D, Porco F, Fiore A (2012b) On the role of equivalent strut models in the seismic assessment of
567 infilled RC buildings. Eng Struct 42:83-94
568 Zuo H, Zhang W, Wang B, Gu X (2021) Seismic behaviour of masonry infilled hinged steel frames with openings:
569 Experimental and numerical studies. Bull Earthq Eng 19:1311-1335

Figures

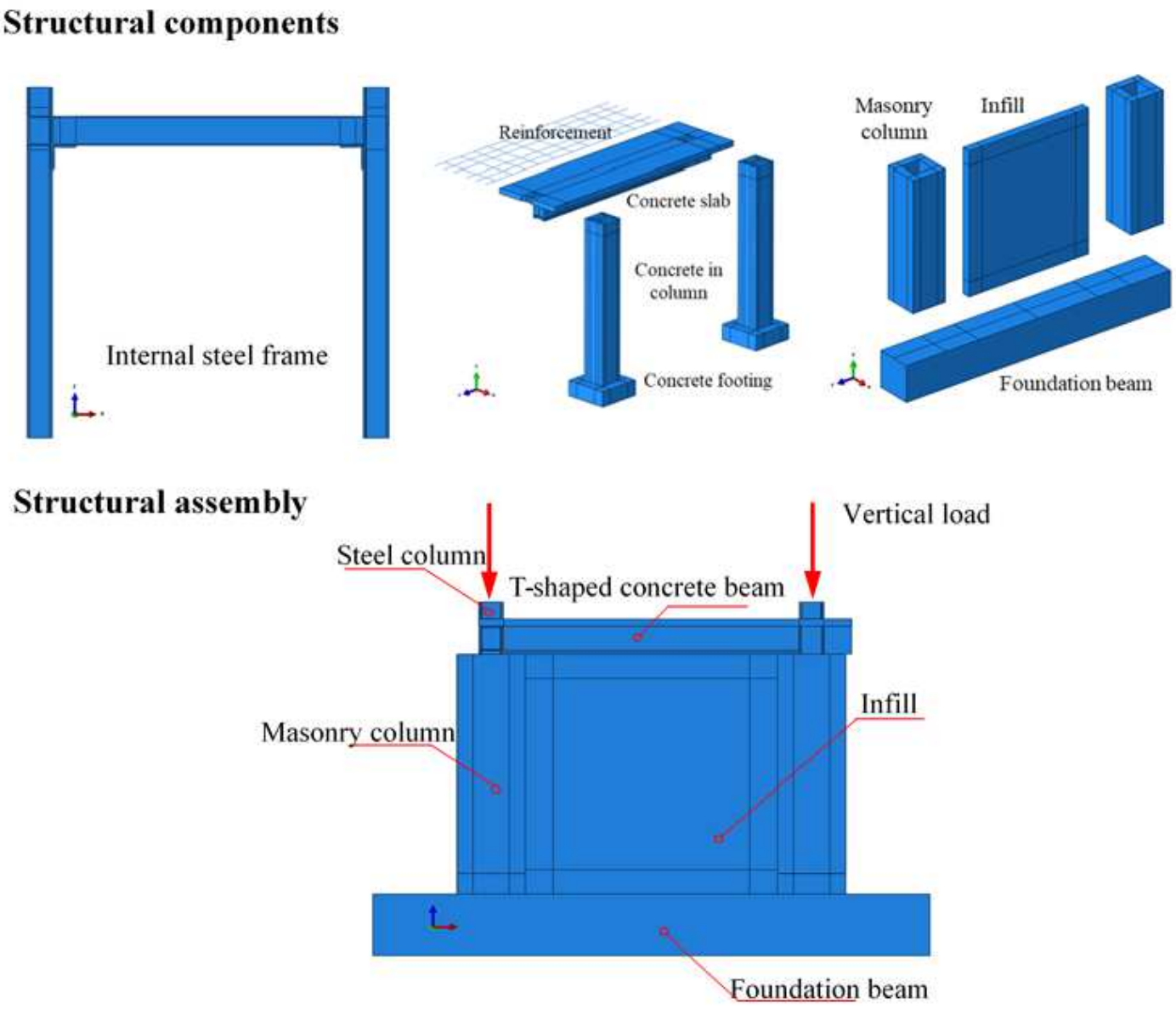

Figure 1

FE model of MIHSFs

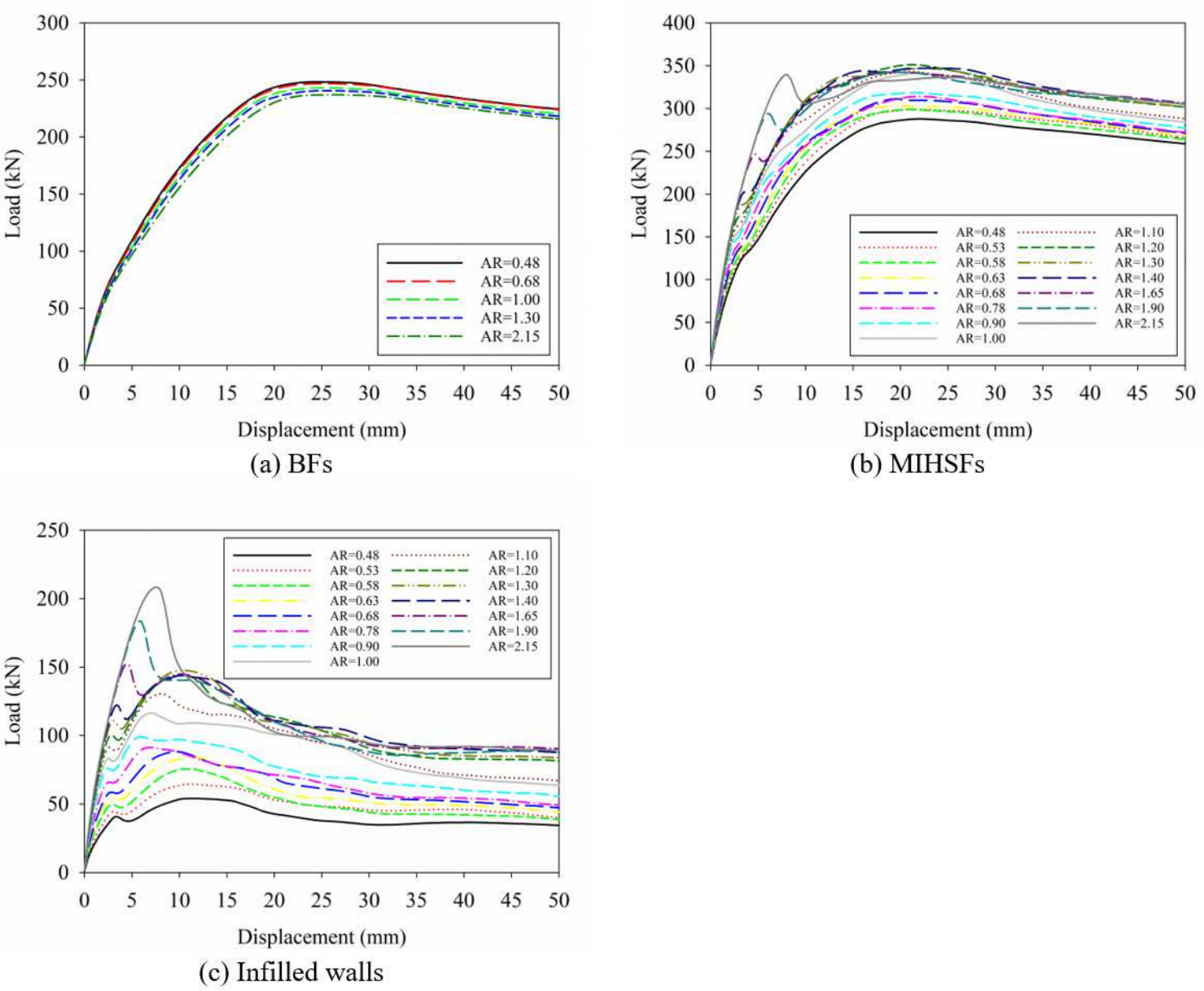

Figure 2

Lateral load-displacement curves of BFs, MIHSFs and infills with different aspect ratios

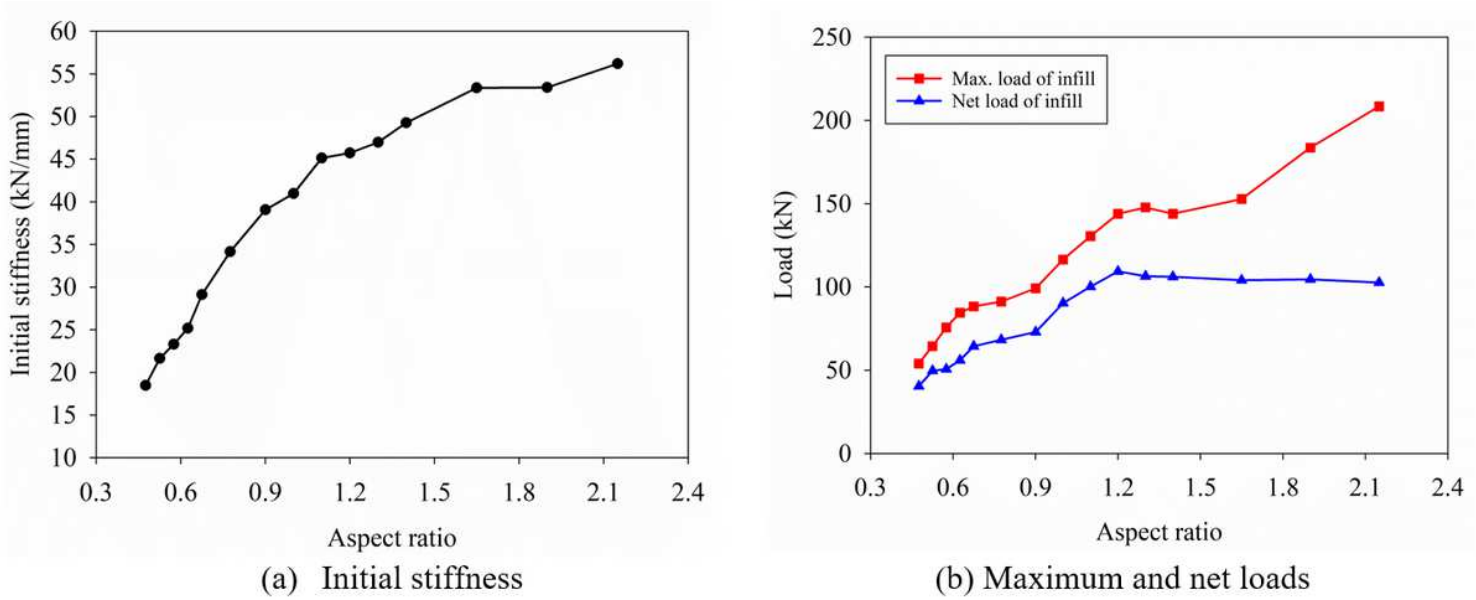

Figure 3

Initial stiffness, maximum and net loads of infills with different aspect ratios

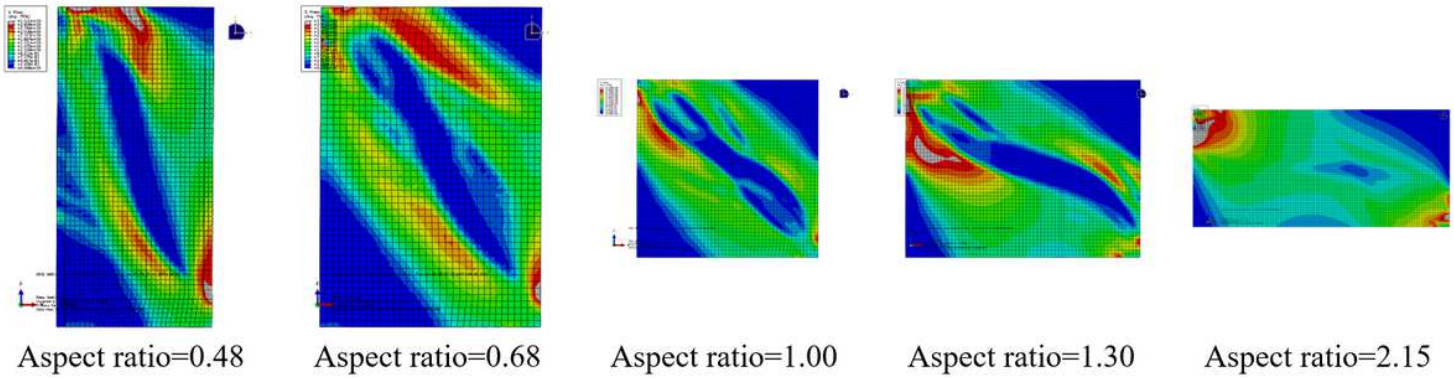

Figure 4

Stress contour of infills with different aspect ratios

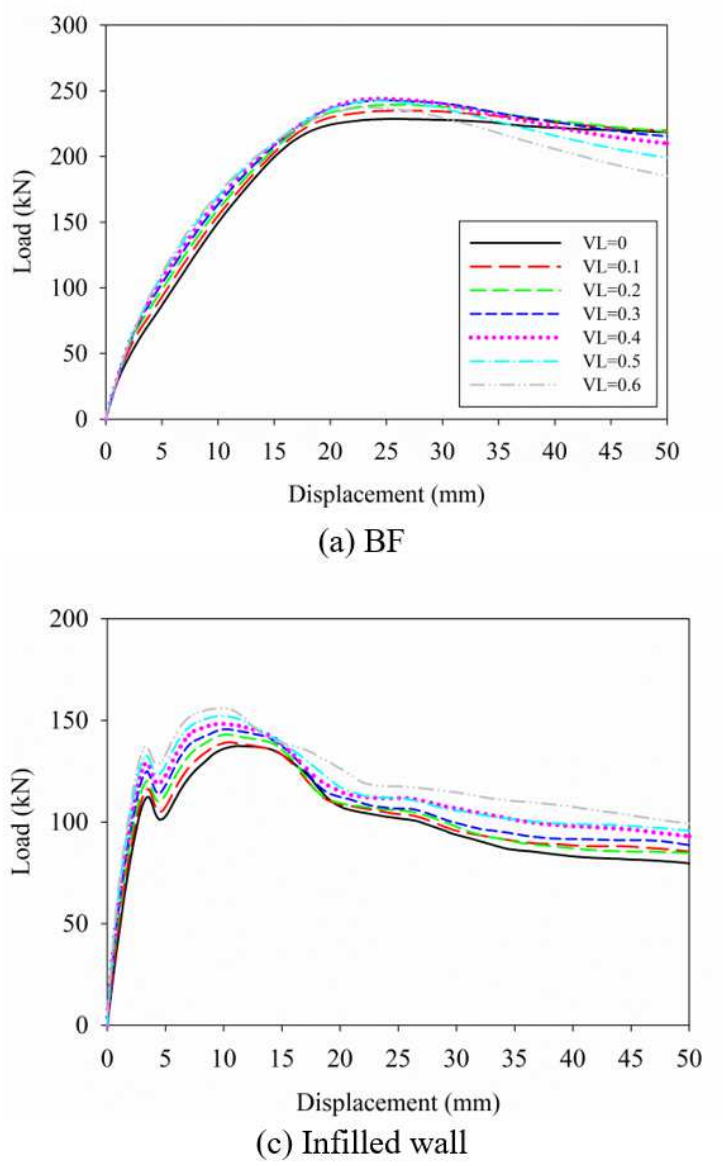

Figure 5

Lateral load-displacement curves of BF, MIHSF and infilled wall under different vertical load levels

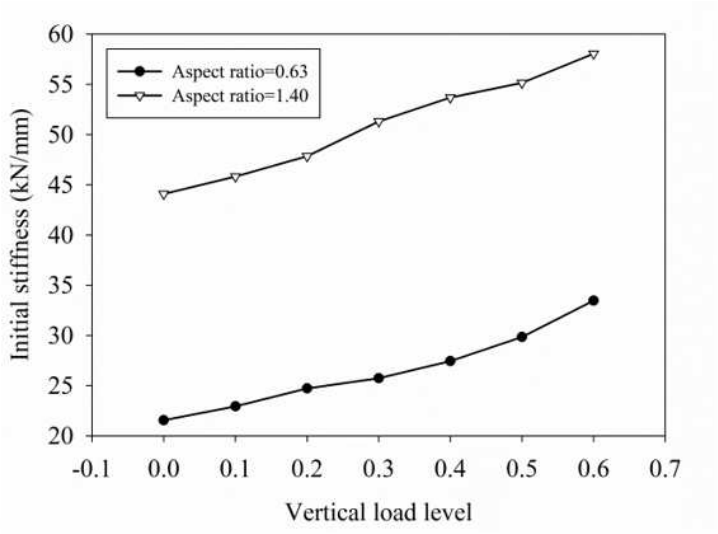

(a) Initial stiffness

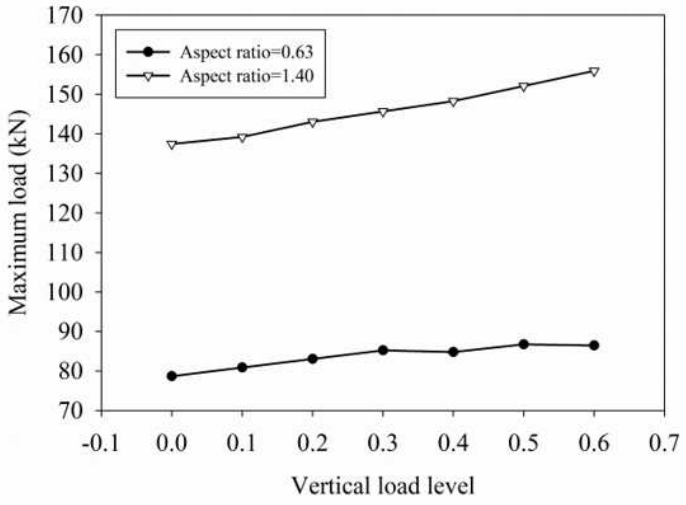

(b) Maximum load

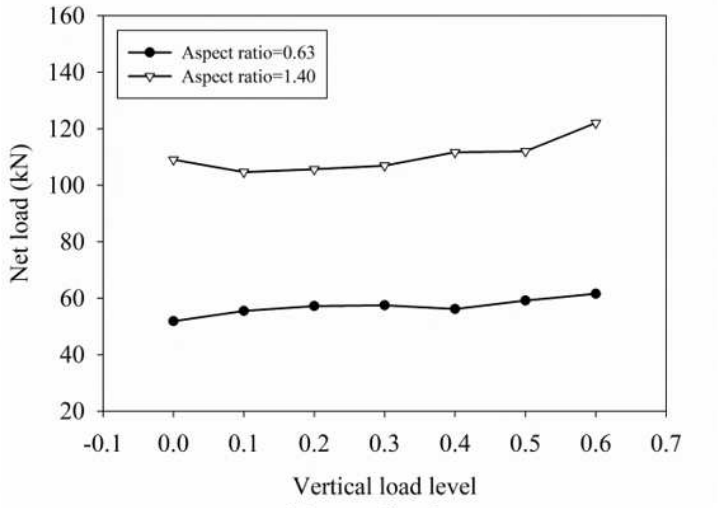

(c) Net load

Figure 6

Initial stiffness, maximum and net loads of infills under different vertical load levels

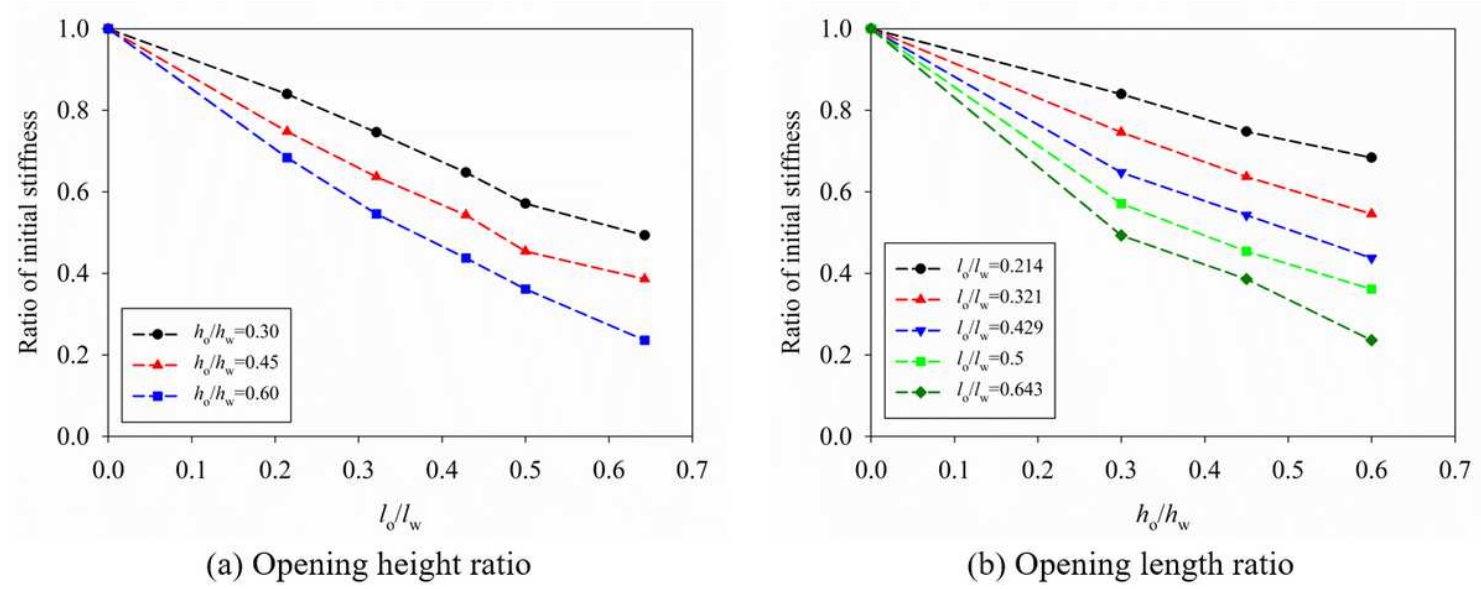

Figure 7

Ratio of initial stiffness of infills with central window openings

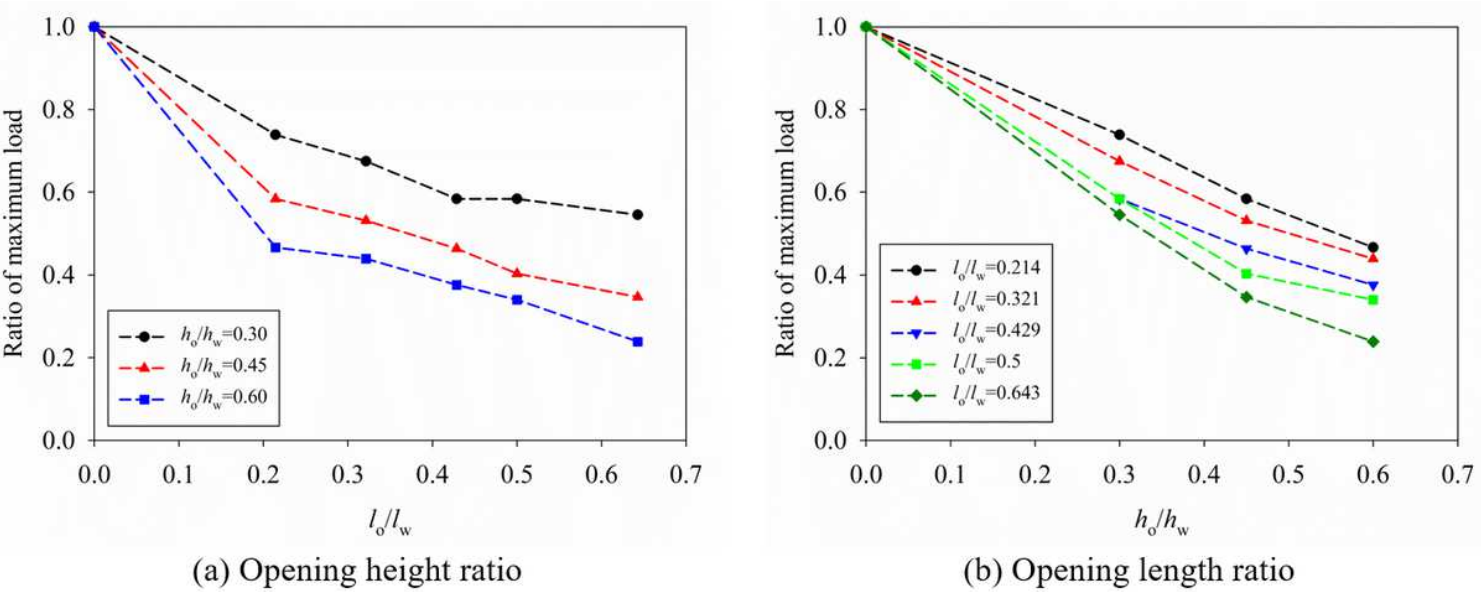

Figure 8

Ratio of maximum lateral load of infills with central window openings

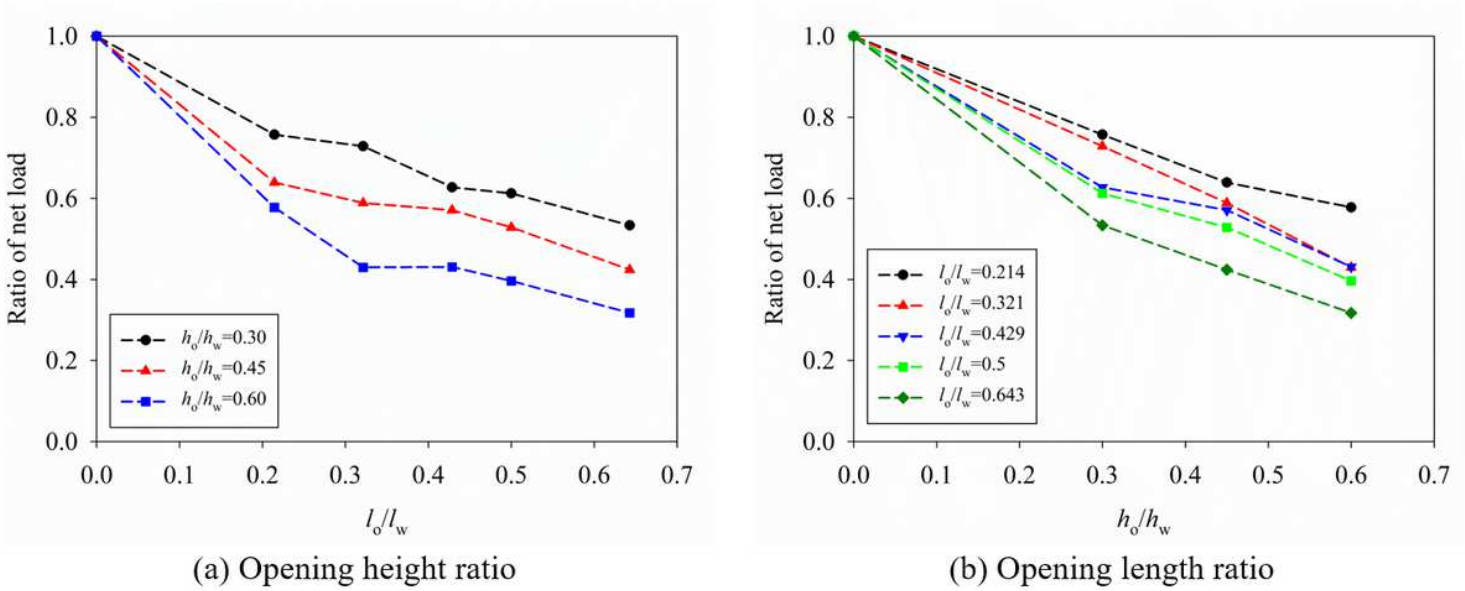

Figure 9

Ratio of net load of infills with central window openings

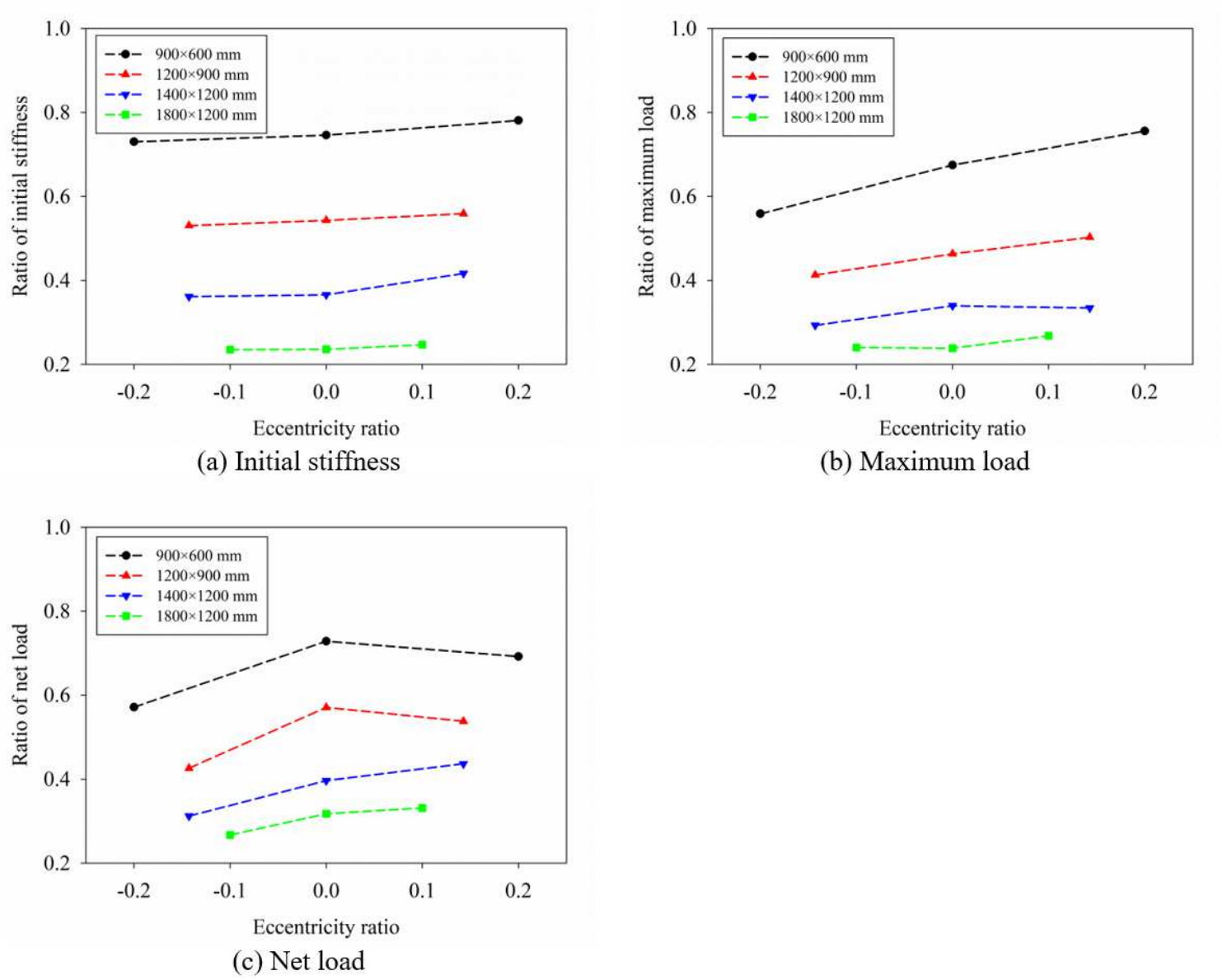

Figure 10

Ratios of stiffness and strength of infills with eccentric window openings

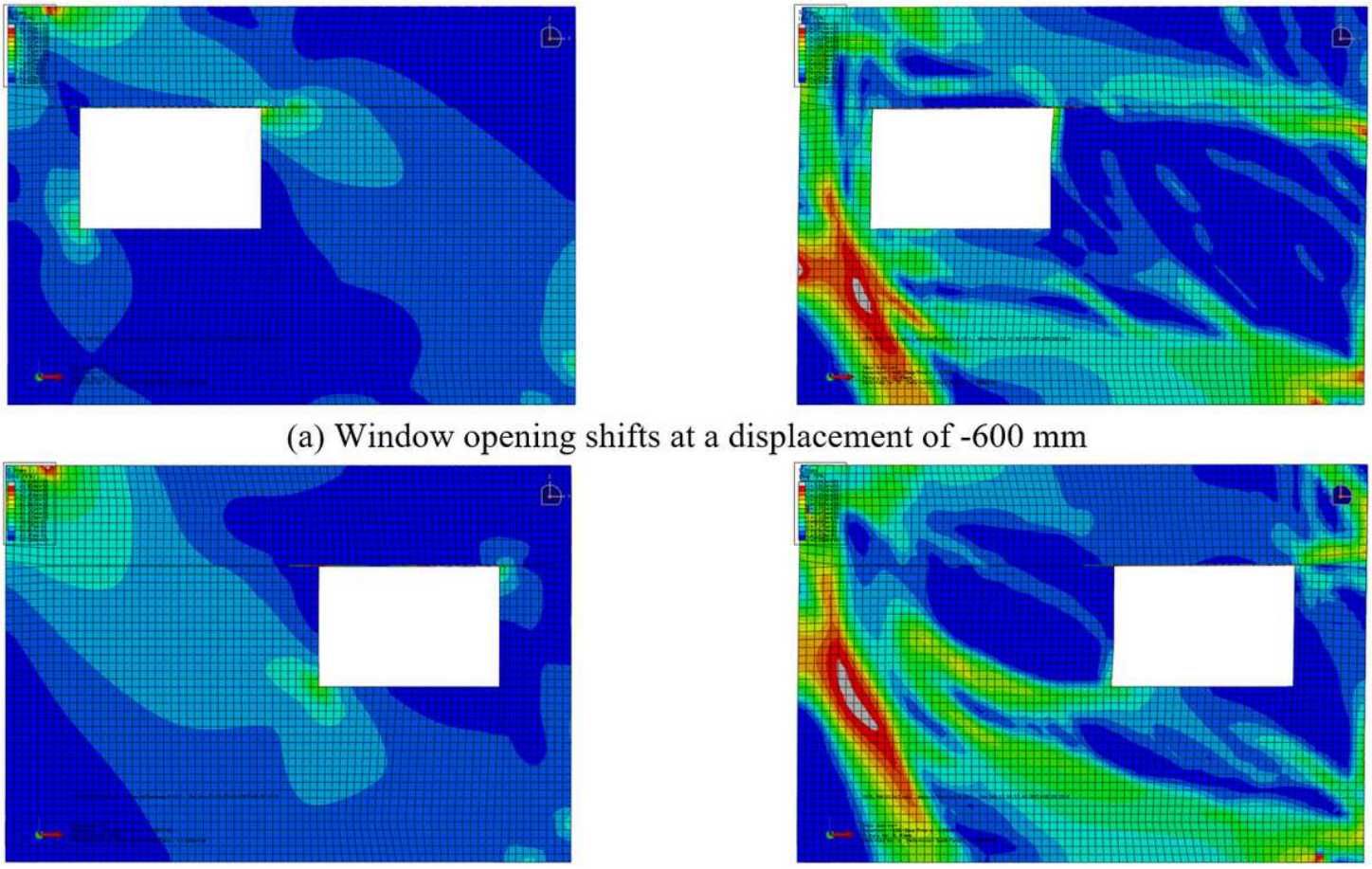

Figure 11

Stress contour of infill with a window opening 900×600 mm

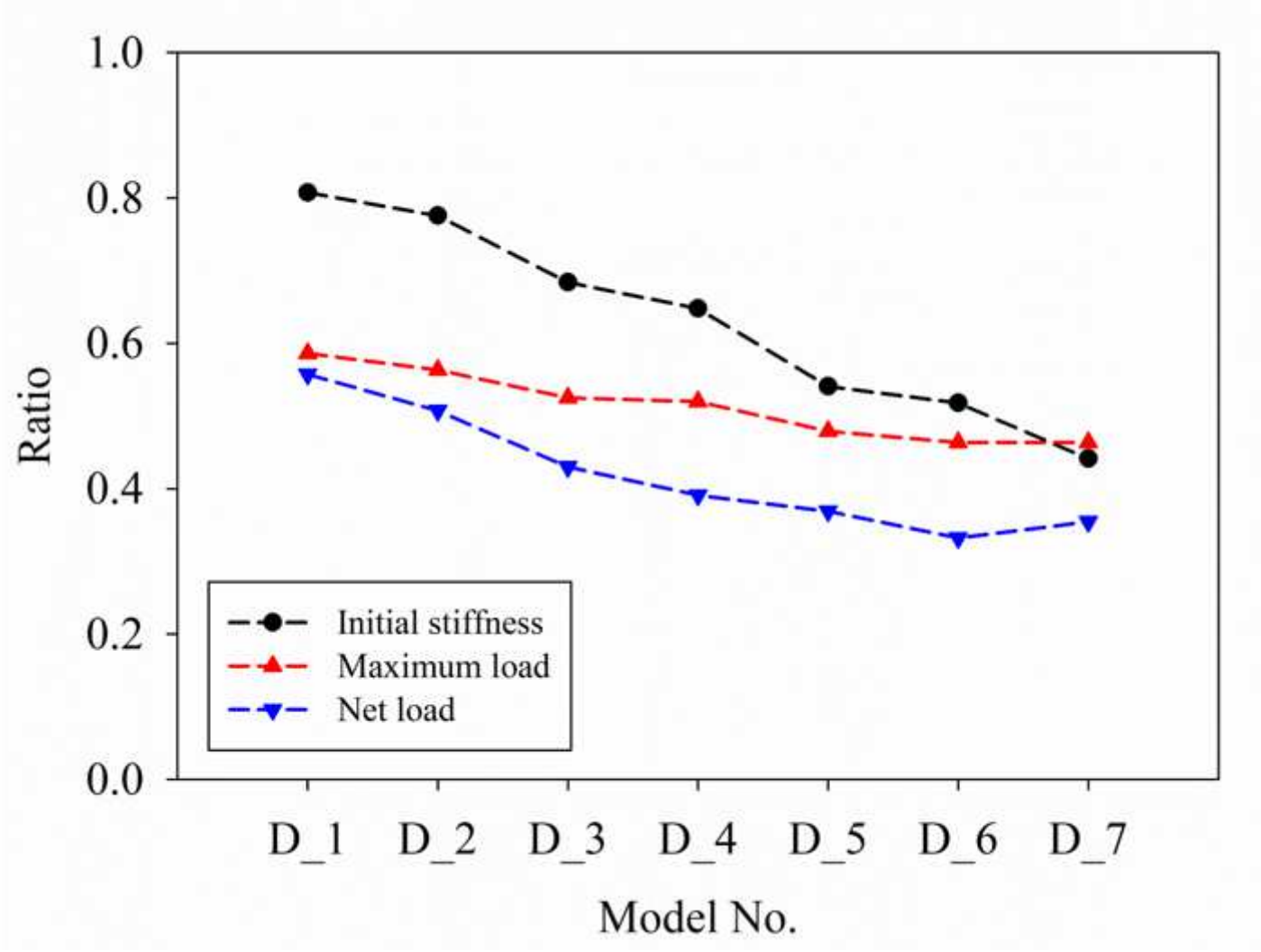

Figure 12

Ratios of stiffness and strength of infills with central door openings

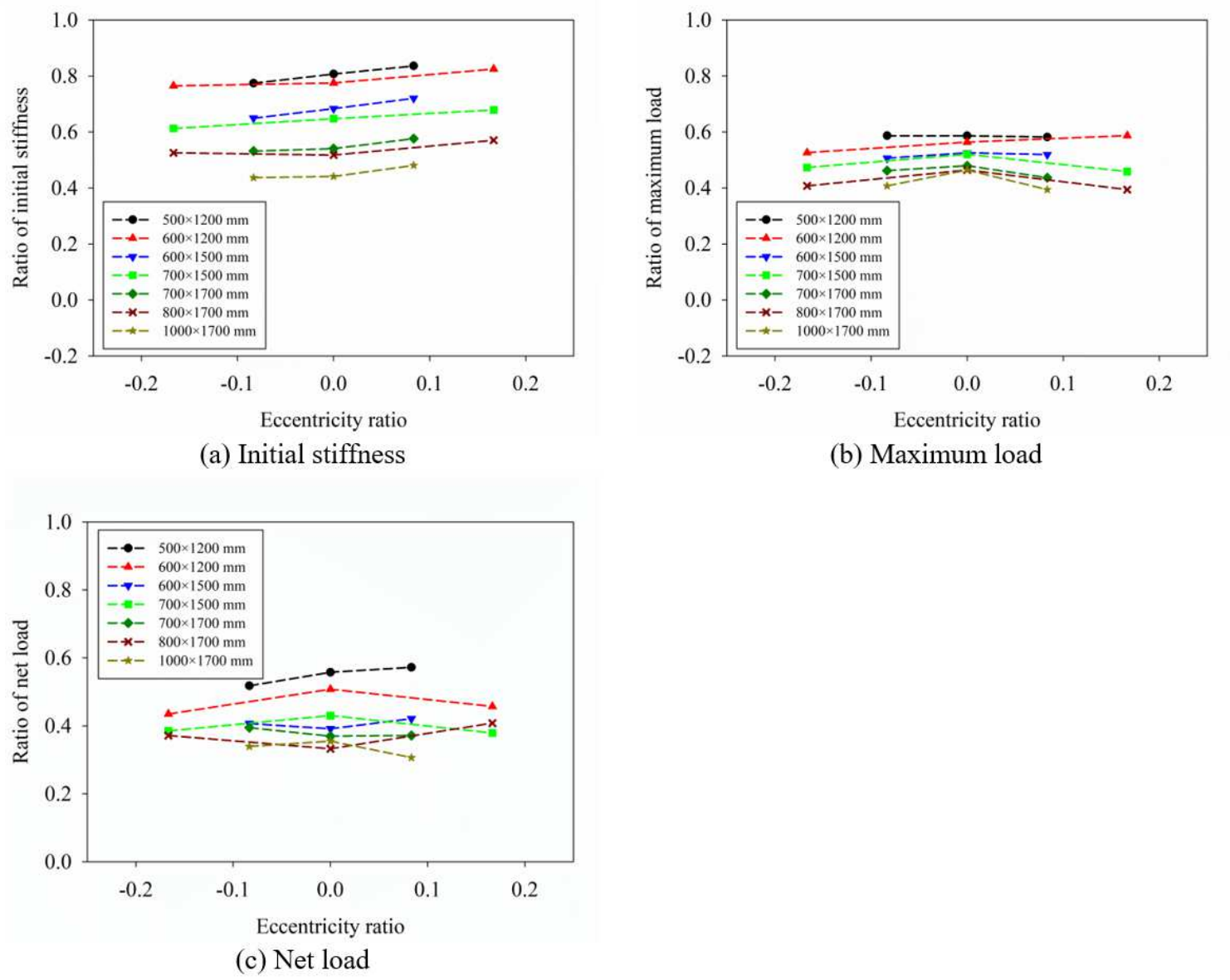

Figure 13

Ratios of stiffness and strength of infills with eccentric door openings

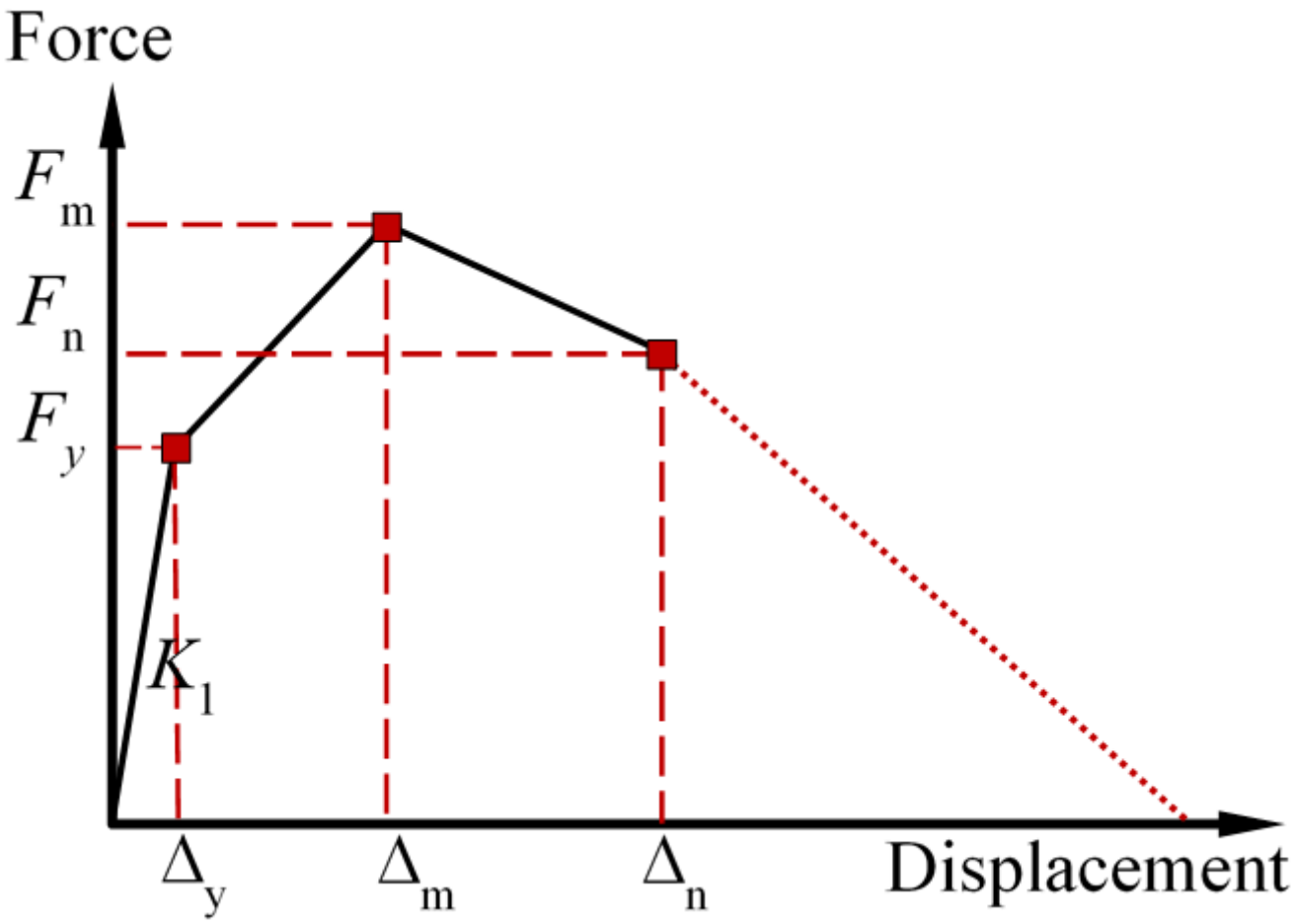

Figure 14

Force-displacement relationship model for solid infills

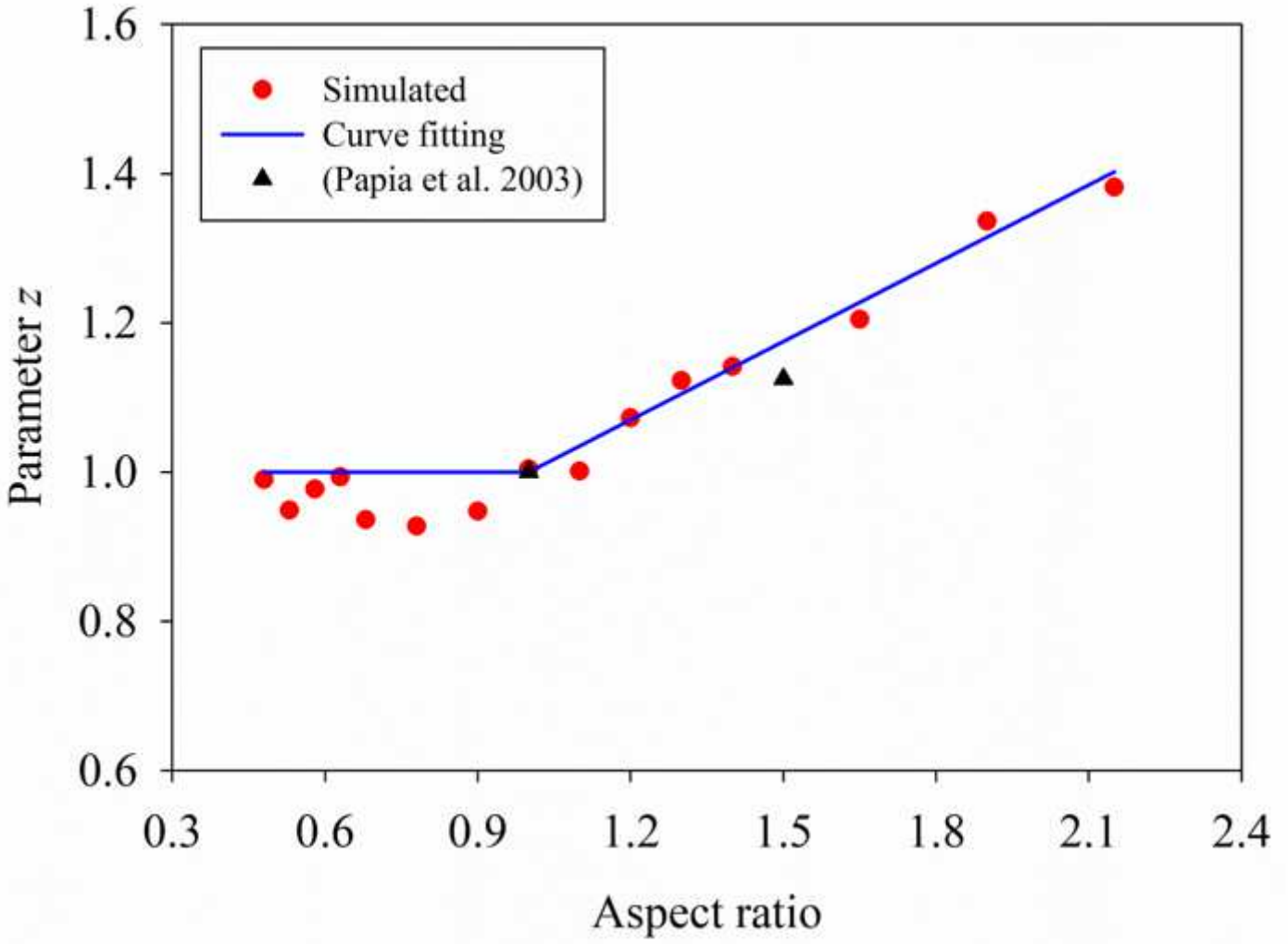

Figure 15

Values of parameter z in Eq. (2) under varying infill aspect ratios

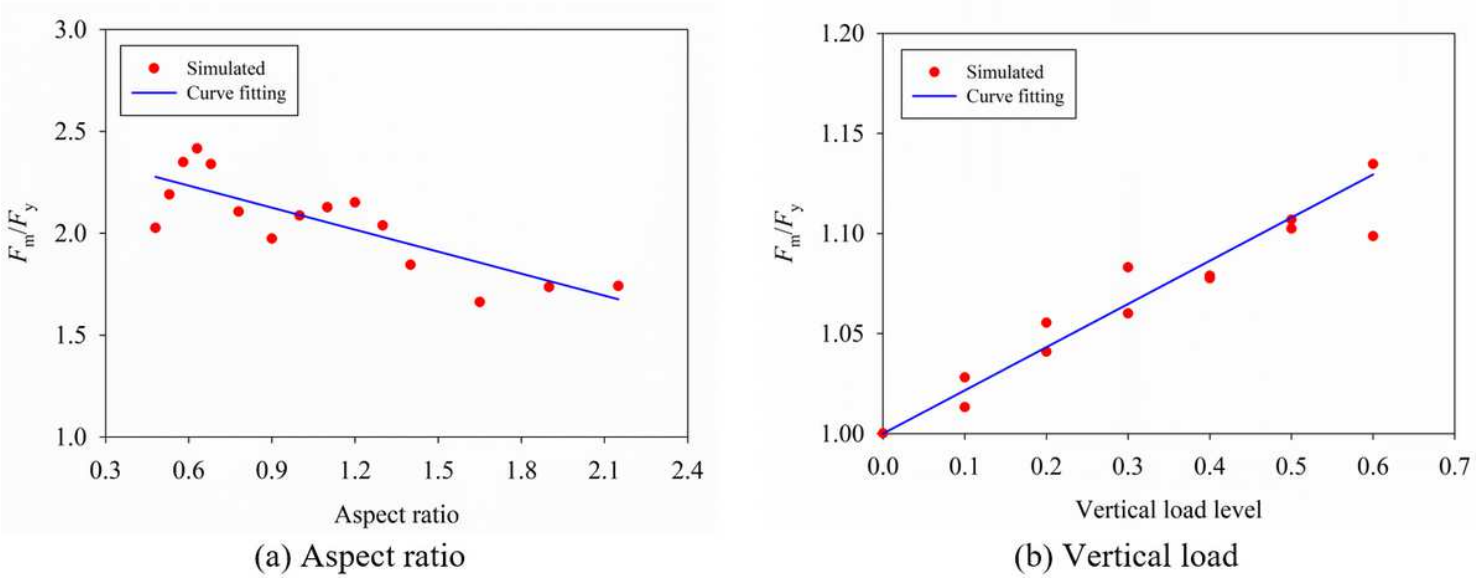

Figure 16

Effects of aspect ratio and vertical load on the maximum lateral load of solid infills

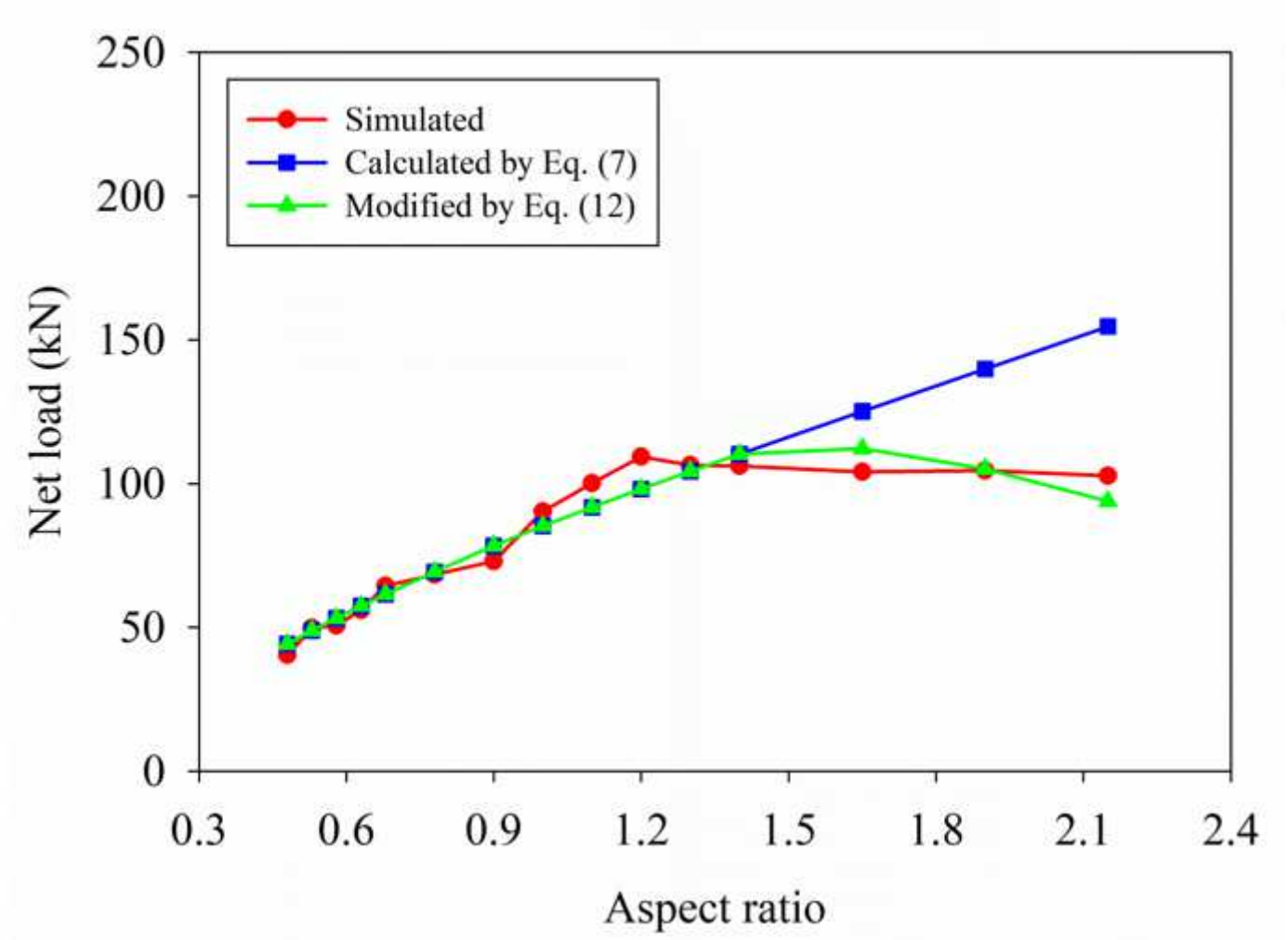

Figure 17

Net loads of solid infills with different aspect ratios

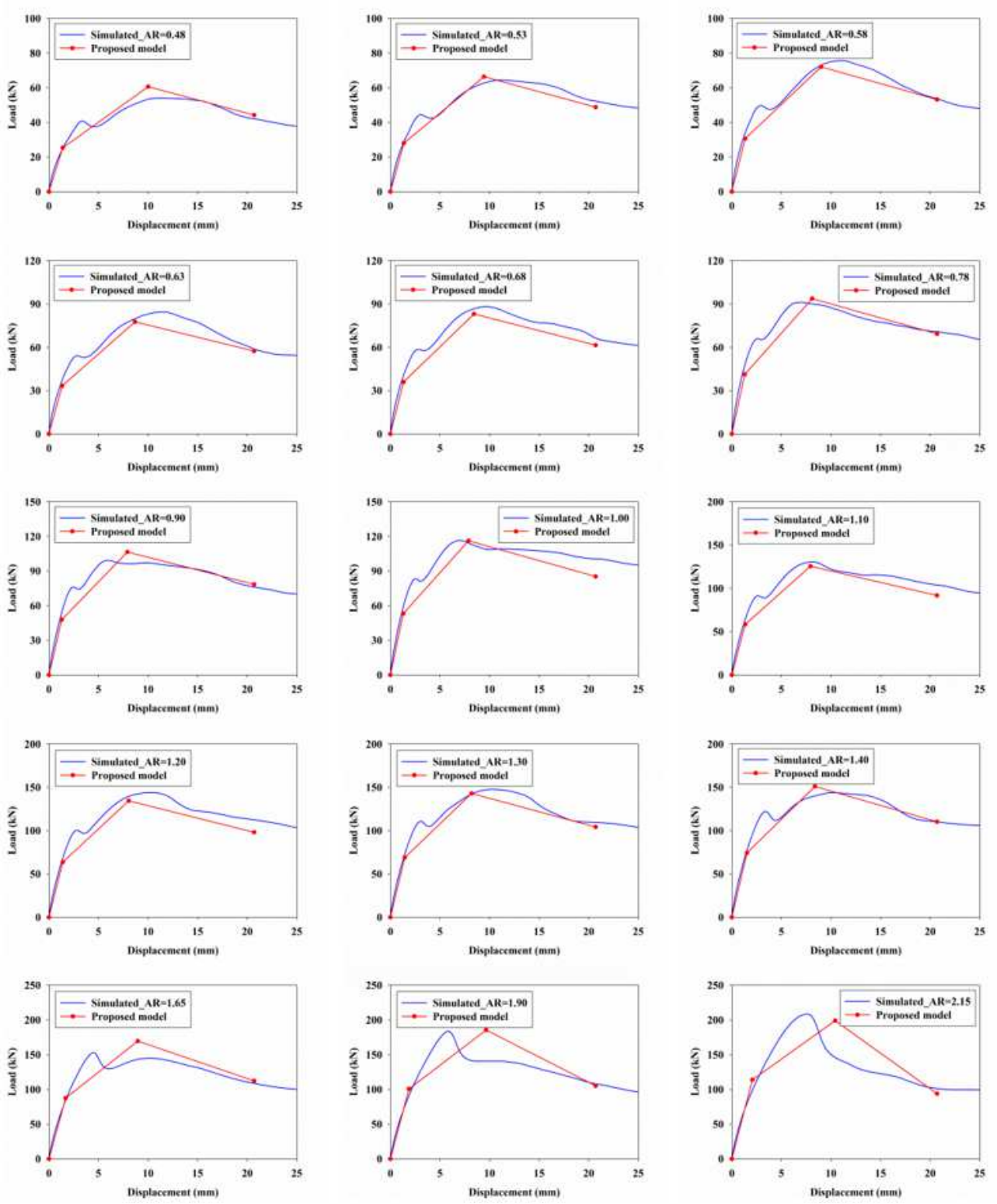

Figure 18

Comparison of force-displacement curves of solid infills with different aspect ratios

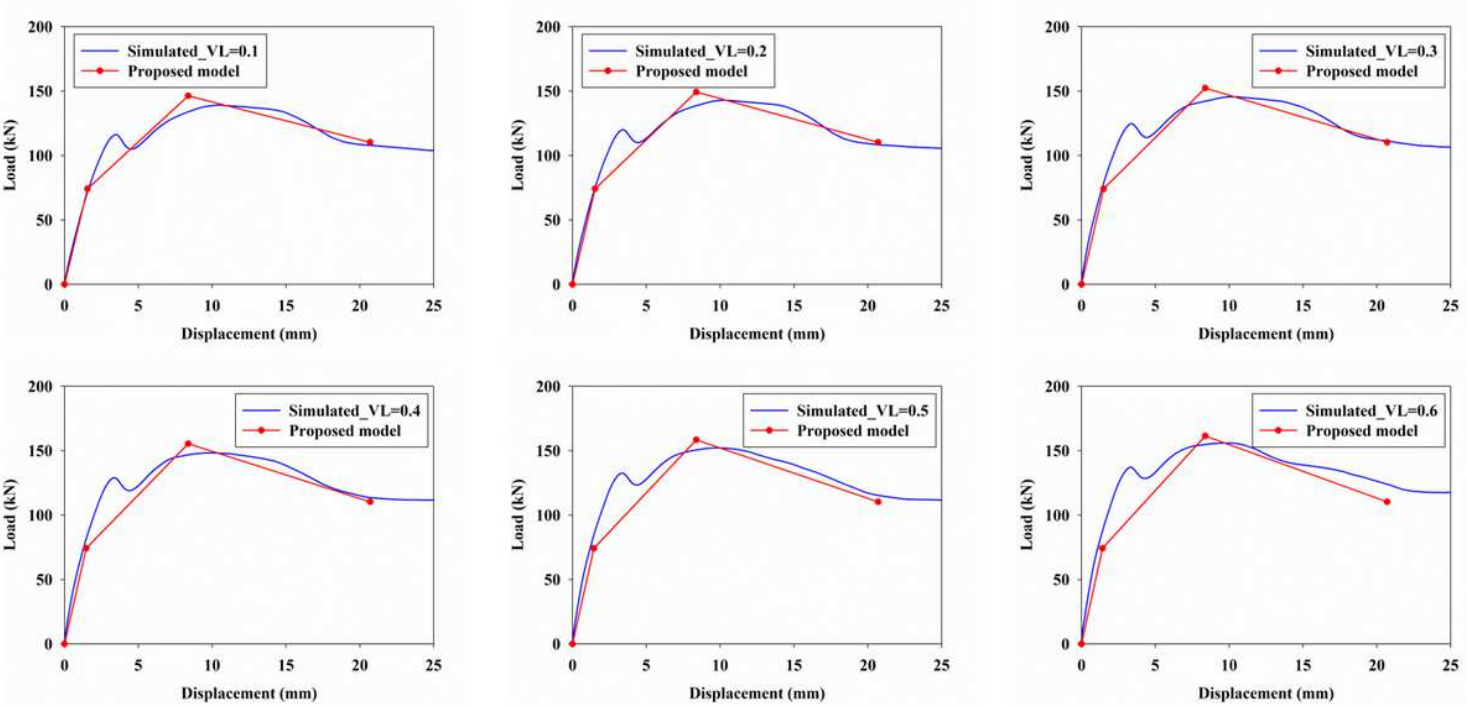

Figure 19

Comparison of force-displacement curves of solid infill under different vertical loads

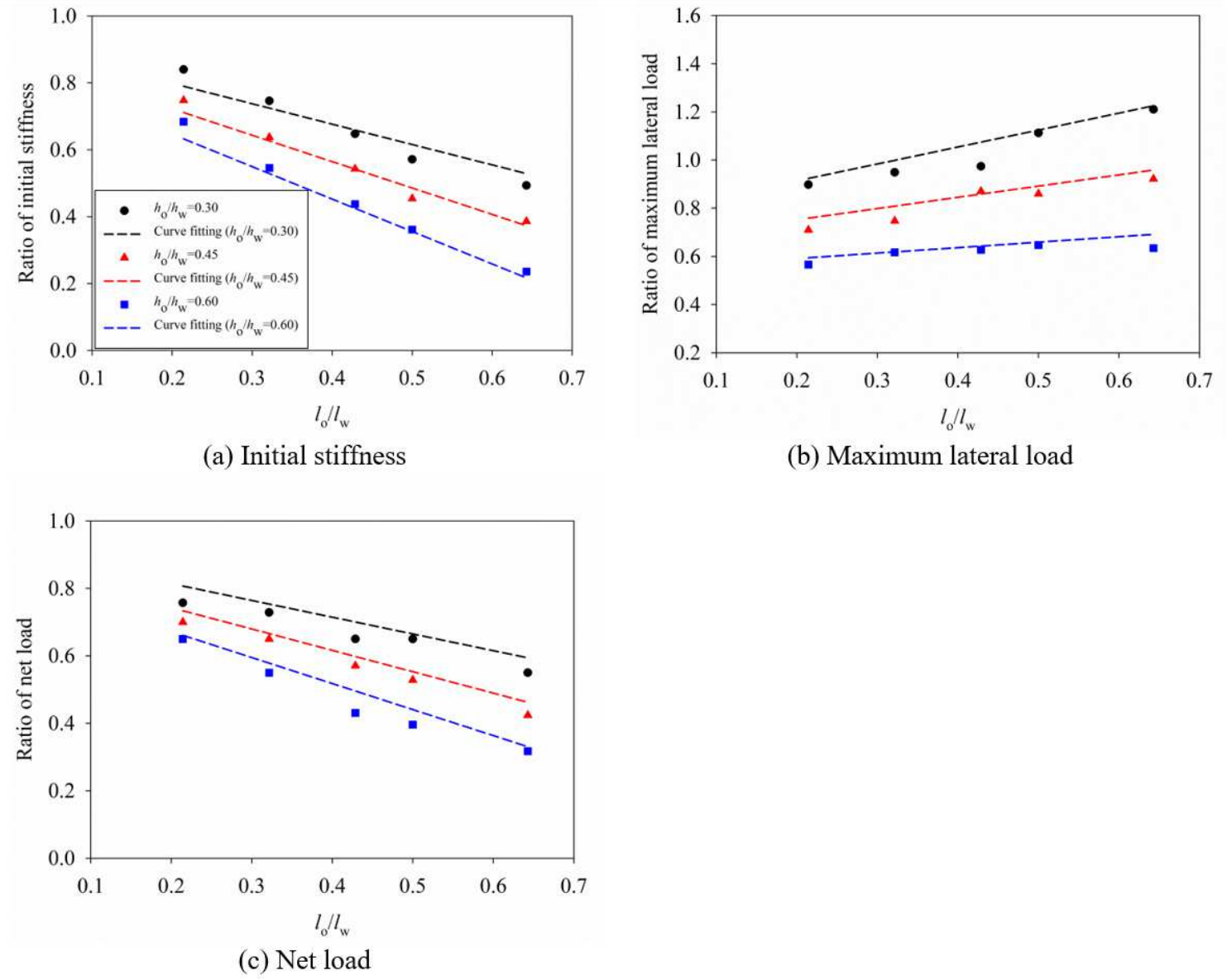

(a) Initial stiffness

(b) Maximum lateral load

(c) Net load

Figure 20

Simulated and calculated ratios of stiffness and strength of infills with window openings

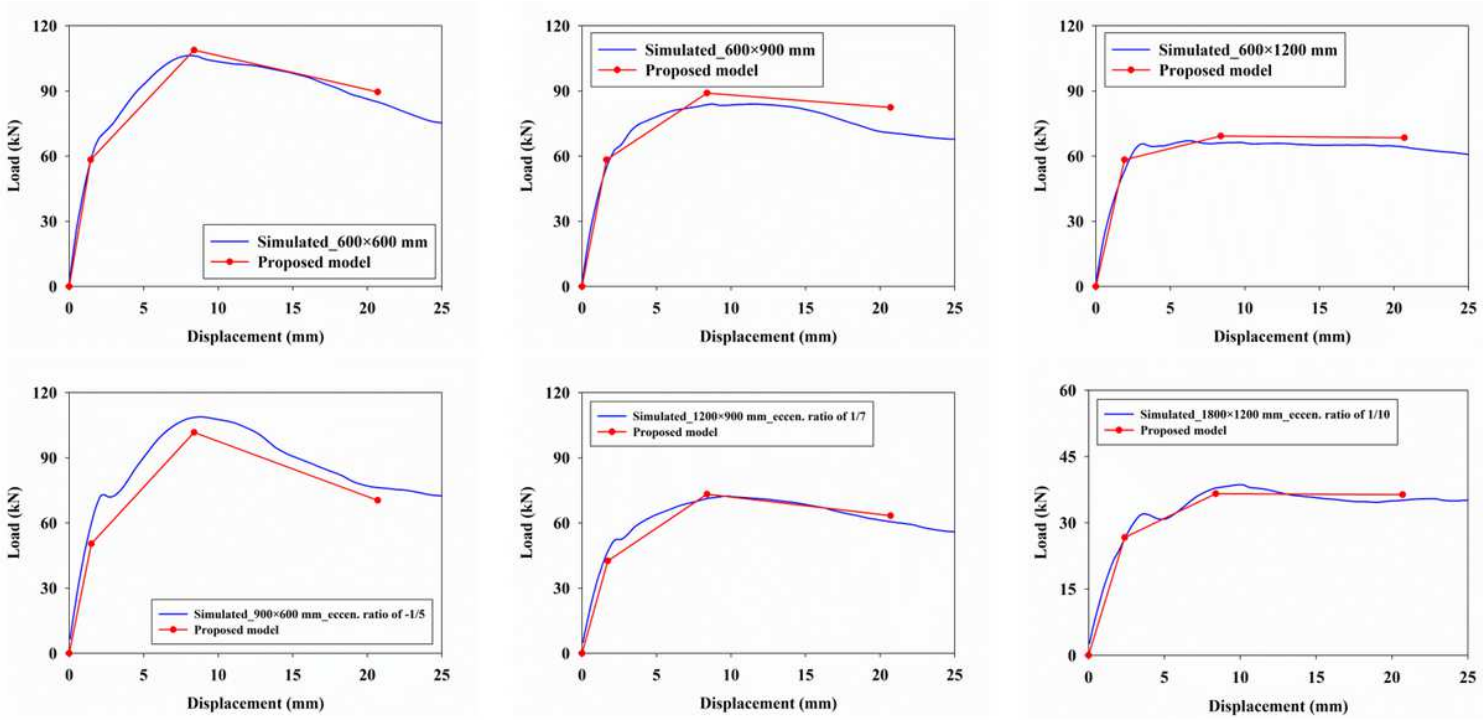

Figure 21

Comparison of force-displacement curves of infills with window openings

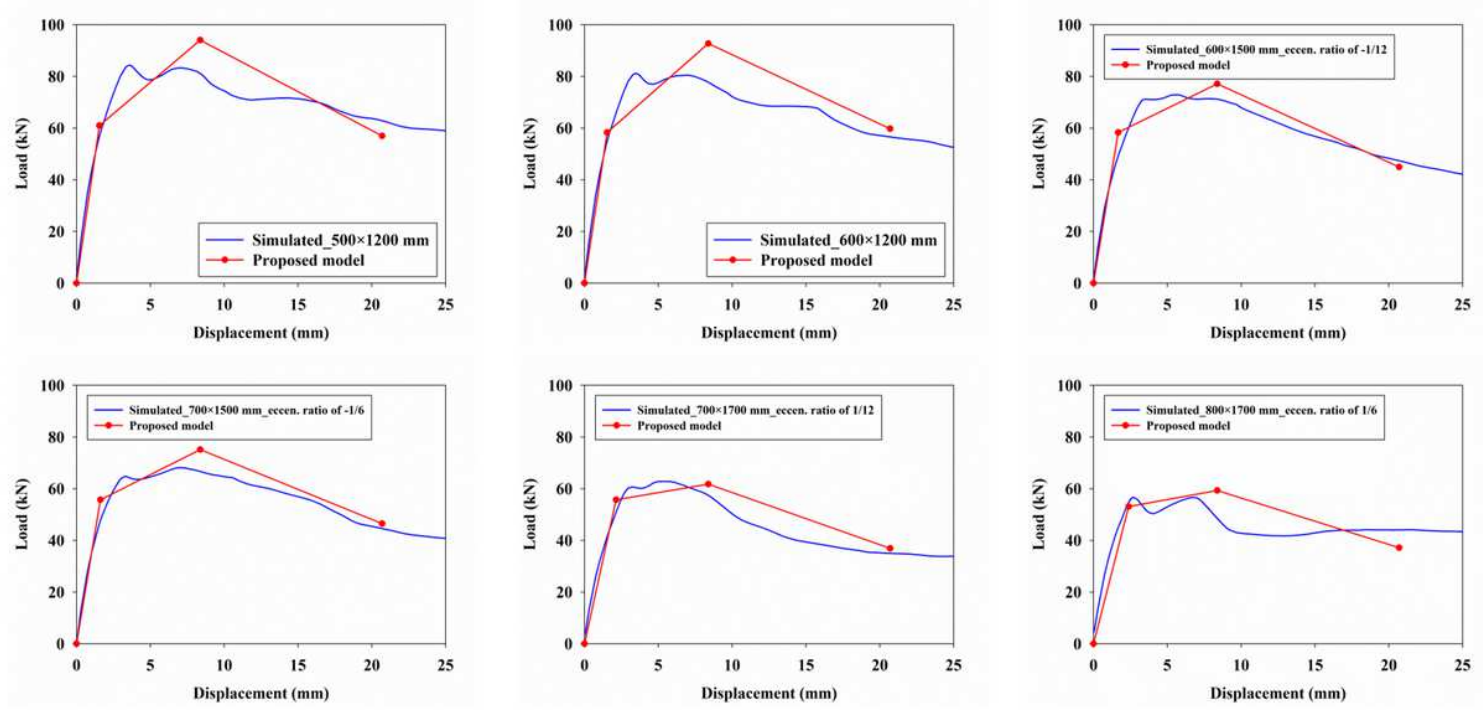

Figure 22

Comparison of force-displacement curves of infills with door openings

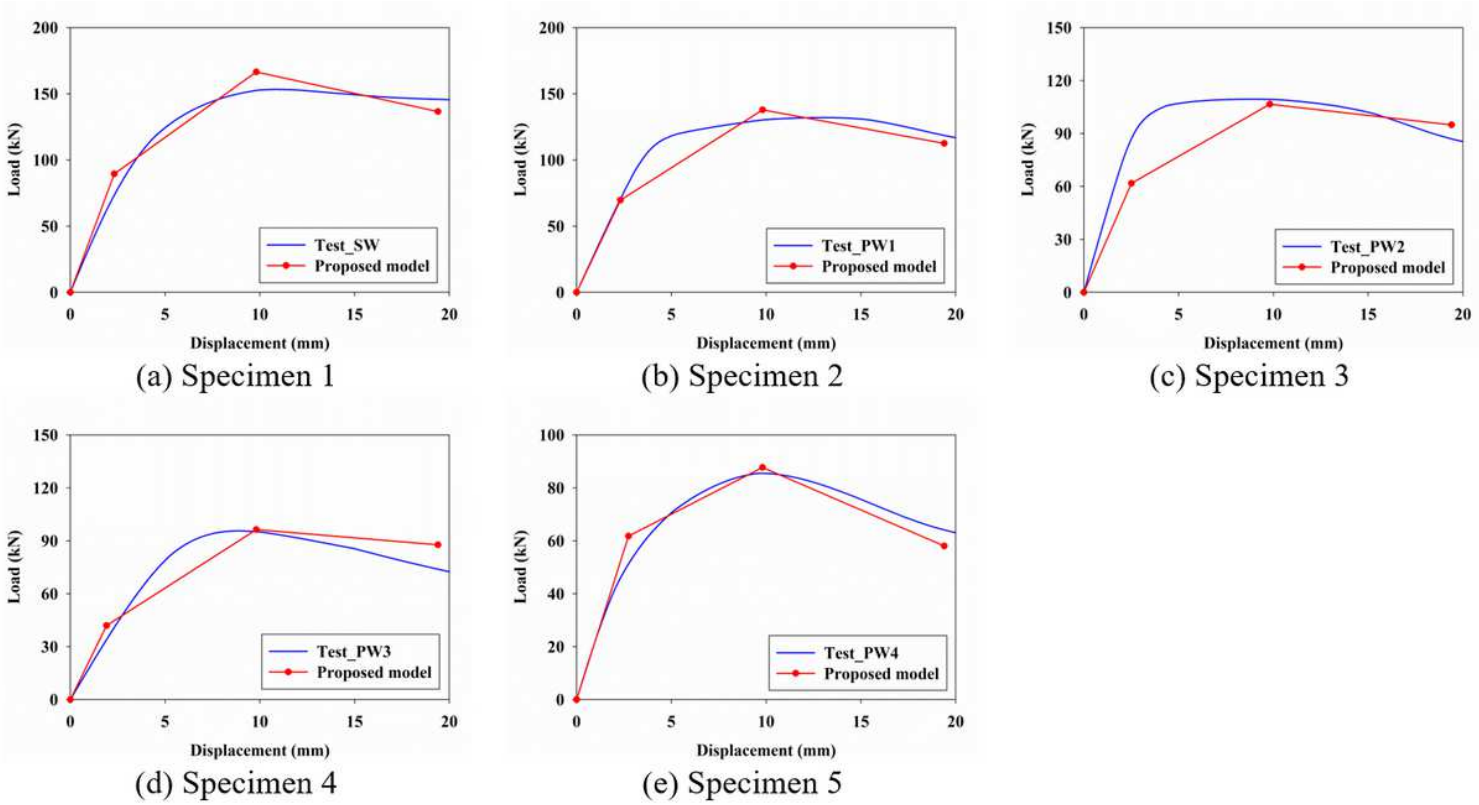

Figure 23

Comparison of force-displacement curves of infills between the proposed model and tests